

Controls on the architectural evolution of deep-water channel overbank sediment wave fields: insights from the Hikurangi Channel, offshore New Zealand

Daniel E. Tek, Adam D. McArthur, Miquel Poyatos-Moré, Luca Colombera, Charlotte Allen, Marco Patacci & William D. McCaffrey

To cite this article: Daniel E. Tek, Adam D. McArthur, Miquel Poyatos-Moré, Luca Colombera, Charlotte Allen, Marco Patacci & William D. McCaffrey (2022) Controls on the architectural evolution of deep-water channel overbank sediment wave fields: insights from the Hikurangi Channel, offshore New Zealand, *New Zealand Journal of Geology and Geophysics*, 65:1, 141-178, DOI: [10.1080/00288306.2021.1978509](https://doi.org/10.1080/00288306.2021.1978509)

To link to this article: <https://doi.org/10.1080/00288306.2021.1978509>



© 2021 The Author(s). Published by Informa UK Limited, trading as Taylor & Francis Group



[View supplementary material](#)



Published online: 04 Oct 2021.



[Submit your article to this journal](#)



Article views: 1446



[View related articles](#)



[View Crossmark data](#)



[Citing articles: 2](#) [View citing articles](#)

Controls on the architectural evolution of deep-water channel overbank sediment wave fields: insights from the Hikurangi Channel, offshore New Zealand

Daniel E. Tek^a, Adam D. McArthur^a, Miquel Poyatos-Moré^b, Luca Colombera^a, Charlotte Allen^c, Marco Patacci^a and William D. McCaffrey^a

^aSchool of Earth and Environment, University of Leeds, Leeds, UK; ^bDepartament de Geologia, Universitat Autònoma de Barcelona, Cerdanyola del Vallés, Spain; ^cShell International Ltd., London, UK

ABSTRACT

Deep-water channels can be bound by overbank deposits, resulting from overspilling flows, which are often ornamented with sediment waves. Here, high-resolution bathymetry, backscatter, and 2D and 3D seismic data are integrated to discern the controls on flow processes on the overbank areas of the Hikurangi Channel. Qualitative seismic interpretation and quantitative analyses of sediment wave morphologies and distributions are conducted through the shallowest 600 m of stratigraphy up to the seafloor. Four outer-bend wave fields are present throughout the studied stratigraphy on the landward margin (left margin looking down-channel) only. Originally closely spaced or combined, these fields evolved to become spatially separated; two of the separate wave fields became further subdivided into distinct outer- and inner-bend fields, whose constituent waves developed distinct differences in morphology and distribution. Sediment wave character is used to interpret the direction and strength of overbank flow. Nine controls on such flow and associated deposition are identified: flow versus conduit size, overbank gradient, flow tuning, Coriolis forcing, contour current activity, flow reflection, centrifugal forcing, interaction with externally derived flows, and interaction of overspill from different locations. Their relative importance may vary across parts of overbank areas, both spatially and temporally, controlling wave field development such that: (1) outer-bend wave fields only develop on the landward margin; (2) the influence of centrifugal force on outer-bend overbanks has increased through time, accompanying a general increase in channel sinuosity; (3) inner-bend wave fields on the landward margin form by the interaction of Coriolis-enhanced inner-bend overbank flow, and outer-bank flow from up-channel bends; (4) inner-bend fields on the oceanward margin form by the interaction of axial flow through wave troughs, and a transverse, toward-channel flow component. This work has implications for interpreting overbank flow from seafloor and seismic data, and for palaeogeographic reconstructions from outcrop data.

ARTICLE HISTORY

Received 17 July 2021
Accepted 6 September 2021

HANDLING EDITOR

Lorna Strachan

KEYWORDS

Overspill; levee; submarine channel; seismic; bathymetry; seafloor; quantitative; sediment waves

Introduction

Deep-water channels are subaqueous conduits through which turbidity currents and other sediment-laden flows transport sediment (Normark 1970), which can contain pollutants (Kane et al. 2020; Zhong and Peng 2021), organic carbon (Hage et al. 2020), fresh water (Kao et al. 2010), and nutrients (Heezen et al. 1955), to the deep seas. Turbidity currents thicker than the depth of the channel they traverse spill onto their overbank areas, depositing fine-grained ‘overbank’ sediments from dilute flows (Piper and Normark 1983). Overbank deposits are accumulations of sediments that can reach almost one thousand metres in thickness and tens of kilometres in width (Pirmez and Flood 1995; Nakajima and Kneller 2013). These deposits can provide a more complete depositional record of channel

evolution than deposits formed on the floors of palaeo-channels, which are susceptible to being excavated by repeated episodes of incision (Morris et al. 2014). Previous studies have led to the development of models of overbank flow and architecture evolution in which progressive trends of diminishing grain size (typically from fine sand to mud) and deposit thickness are seen in transects away from the levee crest (Kane et al. 2007; Morris et al. 2014). However, these simple trends may be complicated by the influence of factors such as: variations in the size of turbidity currents relative to their host conduit (Dennielou et al. 2006), flow ‘tuning’ (Mohrig and Buttles 2007; Kelly et al. 2019), variations in overbank slope gradient (Kane et al. 2010; Nakajima and Kneller 2013), sinuosity (Timbrell 1993; Kane et al. 2008), structural confinement (Clark and Cartwright 2011), the Coriolis

CONTACT Daniel E. Tek  ee11dt@leeds.ac.uk

 Supplemental data for this article can be accessed <https://doi.org/10.1080/00288306.2021.1978509>.

© 2021 The Author(s). Published by Informa UK Limited, trading as Taylor & Francis Group
This is an Open Access article distributed under the terms of the Creative Commons Attribution-NonCommercial-NoDerivatives License (<http://creativecommons.org/licenses/by-nc-nd/4.0/>), which permits non-commercial re-use, distribution, and reproduction in any medium, provided the original work is properly cited, and is not altered, transformed, or built upon in any way.

force (Klaucke et al. 1998; Cossu et al. 2015), and contour currents (Fuhrmann et al. 2020; Miramontes et al. 2020).

Channel overbank areas are often ornamented with sediment waves. Sediment waves are undulating bedforms that are commonly observed on the modern seafloor in a range of sedimentary environments (see Wynn and Stow 2002; Symons et al. 2016). The crests of sediment waves on channel overbanks are typically orientated parallel to the slope contours (Wynn and Stow 2002), meaning they can range in orientation from parallel (e.g. Nakajima and Satoh 2001) to perpendicular to their adjacent channel (e.g. Kuang et al. 2014). In crest-perpendicular transects overbank sediment waves have distinct stoss (upstream) sides that typically dip toward the channel and lee (downstream) sides that dip away from the channel, and typically exhibit wavelengths up to 7 km and heights up to 80 m (Wynn and Stow 2002). They are found adjacent to reaches of channels that may extend hundreds of kilometres (e.g. Damuth 1979; Migeon et al. 2004), and form fields that can extend for tens of kilometres (laterally) away from their formative channel (e.g. Normark et al. 1980; Carter et al. 1990). The upstream migration of sediment waves generates quasi-sinusoidal geometries commonly observed in seismic data imaging sediments beneath sediment wave fields. These depositional geometries can be present through hundreds of metres of stratigraphy (e.g. Migeon et al. 2000, 2001; Nakajima and Satoh 2001). Two models have been proposed to explain the generation of such geometries: (a) flows with uniformly low Froude numbers, wherein increases in near-bed shear stresses on the lee sides inhibits deposition (the 'lee wave model'; Flood 1988; Figure 1A); or (b) flows with variable Froude numbers, wherein supercritical flow on the lee sides of the waves inhibits deposition, and a transition to subcritical flow occurs on the stoss side, essentially making the waves 'cyclic-steps' (Slootman and Cartigny 2020; Figure 1B).

It is commonly inferred that the crests of overbank sediment waves are orientated subperpendicular to the dominant local flow direction (Nakajima et al. 1998; Migeon et al. 2000), and their wavelengths and heights scale with the thickness, and velocity, of the

overspilling flows that formed them (Normark et al. 2002). Therefore, the morphology of sediment waves can be valuable in inferring the dynamics of overspilling flow from modern deep-water channels (Normark et al. 1980, 2002). However, a lack of high-resolution, 3D seismic data imaging deep-water overbank deposits has hitherto inhibited analysis of their architectures and morphological analysis of buried sediment waves. This has hindered the capacity to infer the nature of, and controls upon, ancient overbank flow dynamics, and how the importance of different controls may change through time.

Here, high-resolution bathymetry, and 2D and 3D seismic data, that image the seafloor geomorphology and subsurface architecture of the Hikurangi Channel and its overbanks, offshore New Zealand, are integrated to address this knowledge gap. This contribution complements Tek et al. (2021), which detailed the channel evolution; the focus here is on the overbank areas. Lewis and Pantin (2002) described the seafloor expression of the Hikurangi Channel and its overbanks, using swath bathymetry and backscatter data. They interpreted centrifugal force, the Coriolis force, and the action of bottom currents as controls on flow dynamics on the overbanks. They also performed a subsurface interpretation, based on 2D seismic data and shallow (<5 m) cores, but did not possess 3D constraint to speculate on the evolution of the wave fields. This study aims to: (a) determine the controls on overbank flow processes, deposition, and resultant depositional architectures, through ~600 m of overbank stratigraphy, and compare these controls with those invoked by Lewis and Pantin (2002); (b) determine how these controls interact with one another, constraining the spatial variability of their influence, and how their relative importance has changed through the depositional period; (c) discern the origin of enigmatic wave-like features on inner-overbanks of channel bends. The objectives of this study are to: (a) characterise the seafloor geomorphology and subsurface architecture of the overbank stratigraphy; (b) identify, and categorise different overbank feature types, and interpret their genesis; (c) perform a quantitative analysis of sediment wave morphologies on the seafloor and subsurface stratigraphy. The

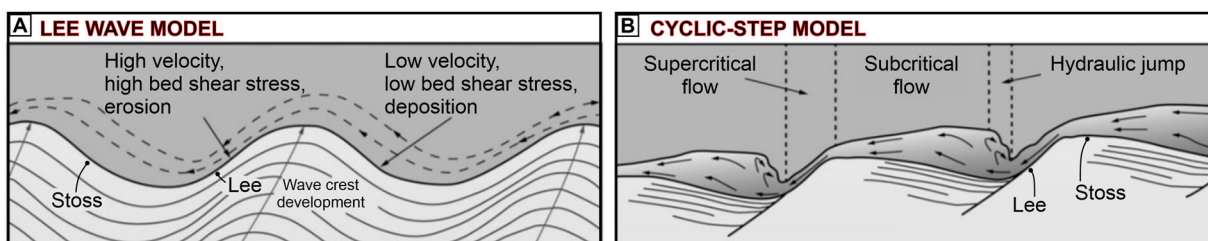


Figure 1. Schematic diagrams showing how sediment waves migrate via **A**, the lee wave model (from Symons et al. 2016; after Flood 1988), and **B**, the cyclic-step model (from Symons et al. 2016; after Cartigny et al. 2011); flow direction is from right to left on both diagrams.

results of this study have fundamental implications for determining controls on the evolution of deep-water channel-levee systems and can facilitate the development of understanding of channel-levee evolution in other modern and ancient systems.

Geological setting

The study area covers $\sim 21,000$ km² of the trench-floor, adjacent to the junction between the Chatham Rise and the subducting Pacific plate, containing a ~ 250 km stretch of the Hikurangi Channel (Figure 2B). This study focuses on the upper ~ 600 m of trench-fill (upper trench fill in Figures 3 and 4), wherein ten channel-forms can be traced for the ~ 140 km length of the 3D seismic survey described in the 'data' section (Tek et al. 2021; Figure 4).

The NE flowing ~ 1800 km long Hikurangi Channel (Figure 2; Lewis and Pantin 2002; Mountjoy et al. 2009, 2018; Tek et al. 2021) sits within the NE-SW oriented Hikurangi Trench, which has developed over the last ~ 27 Ma due to the subduction of the Pacific plate beneath the Australian plate (Ballance 1975; Nicol et al. 2007; Barnes et al. 2010; Lamb 2011; Jiao et al. 2015). Most of the trench-fill has accumulated during the last 3.5 Ma (Figure 3A; Ghisetti et al. 2016; Kroeger et al. 2019), and is interpreted to consist predominantly of turbidites associated with the Hikurangi Channel (Lewis 1994; Lewis et al. 1998; McArthur and Tek 2021) and with transverse drainage networks that traversed the slope and subduction wedge (Figure 2B; Mountjoy et al. 2009; McArthur et al. 2021). In the SW of the trench, where this study is focused, the trench-fill is ~ 6 km thick; the top ~ 600 m of stratigraphy, studied herein (Figure 3), is dominated by overbank deposits from the Hikurangi Channel (McArthur and Tek 2021). To the NE, the trench-fill thins to ~ 1 km (Lewis et al. 1998; Barnes et al. 2010; Plaza-Faverola et al. 2012).

The Hikurangi Channel is fed by a network of shelf-incising canyons that capture sediment from the North and South Islands of New Zealand (Carter 1992; Lewis 1994; Lewis et al. 1998; Lewis and Barnes 1999; Mountjoy et al. 2009), and are flushed by earthquake-triggered failure events (Mountjoy et al. 2018; Howarth et al. 2021). Downstream of the confluence with the Cook Strait Canyon, the Hikurangi Channel flows east along the northern margin of the Chatham Rise (Wood and Davy 1994; Davy et al. 2008) for ~ 130 km (Figure 2). It then runs through the trench for ~ 500 km before abruptly changing direction and continuing a further ~ 1150 km across the Hikurangi Plateau and the Pacific abyssal plain (Figure 2; Lewis et al. 1998; Collot et al. 2001; Lewis and Pantin 2002). In the study area, in the proximal part of the trench, where the channel departs from the Chatham

Rise, the overbank areas of the channel are ornamented by the scars from numerous channel-wall failures (Watson et al. 2020; Tek et al. 2021) and by sediment waves (Lewis et al. 1998; Lewis and Pantin 2002).

A change in the nature of the trench-fill (Figure 3) is observed between ~ 600 and ~ 800 m depth (above R4 in Figure 3), from deeper isolated channel-forms that exhibit significant lateral offsets, to shallower aggradational channel-forms that each follows a similar course to their predecessor (Figure 3A; McArthur and Tek 2021). The stratigraphy of interest is located above this transition, where the trench-fill comprises thick, compound overbank deposits that bound the aforementioned aggradational channel-forms.

Contour currents have been identified in the Hikurangi Trench but their locations and orientations are poorly constrained, and their effects have likely changed through time (Carter et al. 2002; Lewis and Pantin 2002; Fernandez et al. 2018; Bailey et al. 2020). For example, based on seafloor geomorphology and seismic architecture, Lewis and Pantin (2002) inferred that a shallow branch of the Deep Western Boundary Current (DWBC) flowed WNW along the northern edge of the Chatham Rise (Figure 2A). The DWBC is interpreted to generate waves on the oceanward channel margin, and to have been active during glacial periods (Lewis and Pantin 2002). However, modern oceanographic data show that the East Cape Current (ECC) is currently the dominant contour current in the study area (Carter et al., 2002; Fernandez et al. 2018). The ECC flows SW following the subduction front before turning anti-clockwise and crossing the channel near or within the study area (Figure 2A); the exact location of its crossing with the channel is unclear.

Data

Analysis of the seafloor was conducted using high-resolution multibeam bathymetry and backscatter data covering $\sim 47,000$ km² (Figure 2A), collected by the National Institute of Water and Atmospheric Research (NIWA) between 2001 and 2013; the data are provided by New Zealand Petroleum and Minerals (NZPAM) as part of their 2017 datapack. Within the study area (Figure 2B), data from two cruises (TAN1207 and TAN1307 respectively) acquired in 2012 and 2013 using an EM302 multibeam echosounder at 30 kHz with a 25 m grid size, are primarily used (Bland et al. 2014; Figure 2B).

Subsurface analysis was conducted using three seismic datasets acquired by Westerngeco: (a) 2600 km² of pre-stack Kirchhoff depth migrated (broadband) 3D seismic data (acquired in 2017) with a horizontal resolution of ~ 25 m and a vertical resolution of ~ 7 m (values accurate at seafloor; Crisóstomo-Figueroa et al. 2020); (b) depth converted 2D seismic data

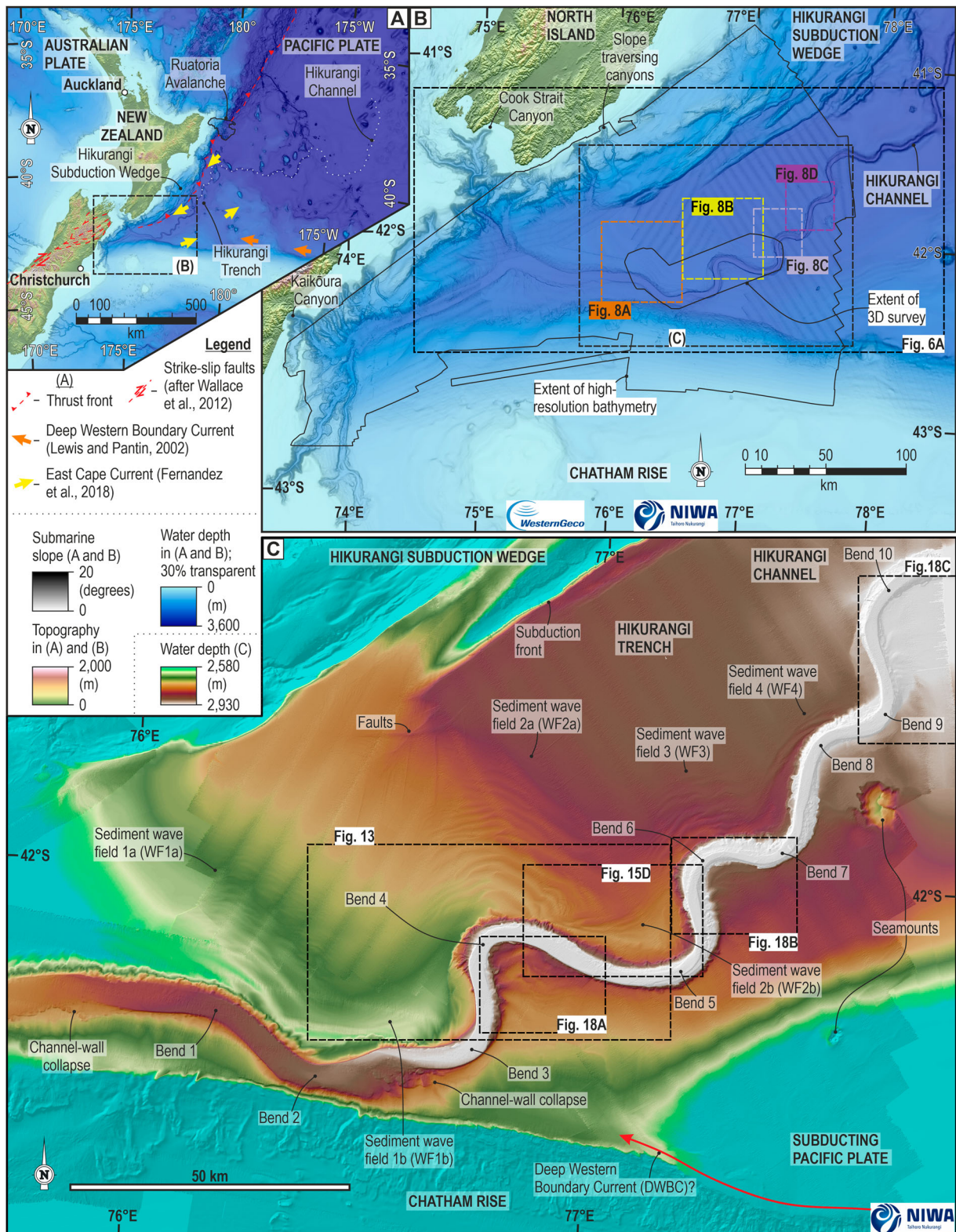


Figure 2. Location maps showing: **A**, the location of the Hikurangi Margin; **B**, the proximal reach of the Hikurangi Channel, showing its relationship with its feeder canyons, the location of the study area slope-traversing trench-perpendicular systems, the location of the study area (see **C**) and the extent of the bathymetry and 3D seismic data used herein; **C**, seafloor morphology in the study area, highlighting the ten channel bends referenced throughout the text, the sediment wave fields on the channel overbanks, and the channels' relationships with the Hikurangi subduction wedge, the Chatham Rise, and the Pacific Plate. Bathymetry data were provided by the New Zealand National Institute for Water and Atmosphere (NIWA) and WesternGeco.

(3–200 Hz frequency), acquired in 2014; (c) time-domain 2D seismic data (30–40 Hz frequency), acquired in 2009. Full-stack data are displayed SEG

positive; a downward decrease in acoustic impedance is shown as a trough (white reflection). All presented seismic sections are shown in depth.

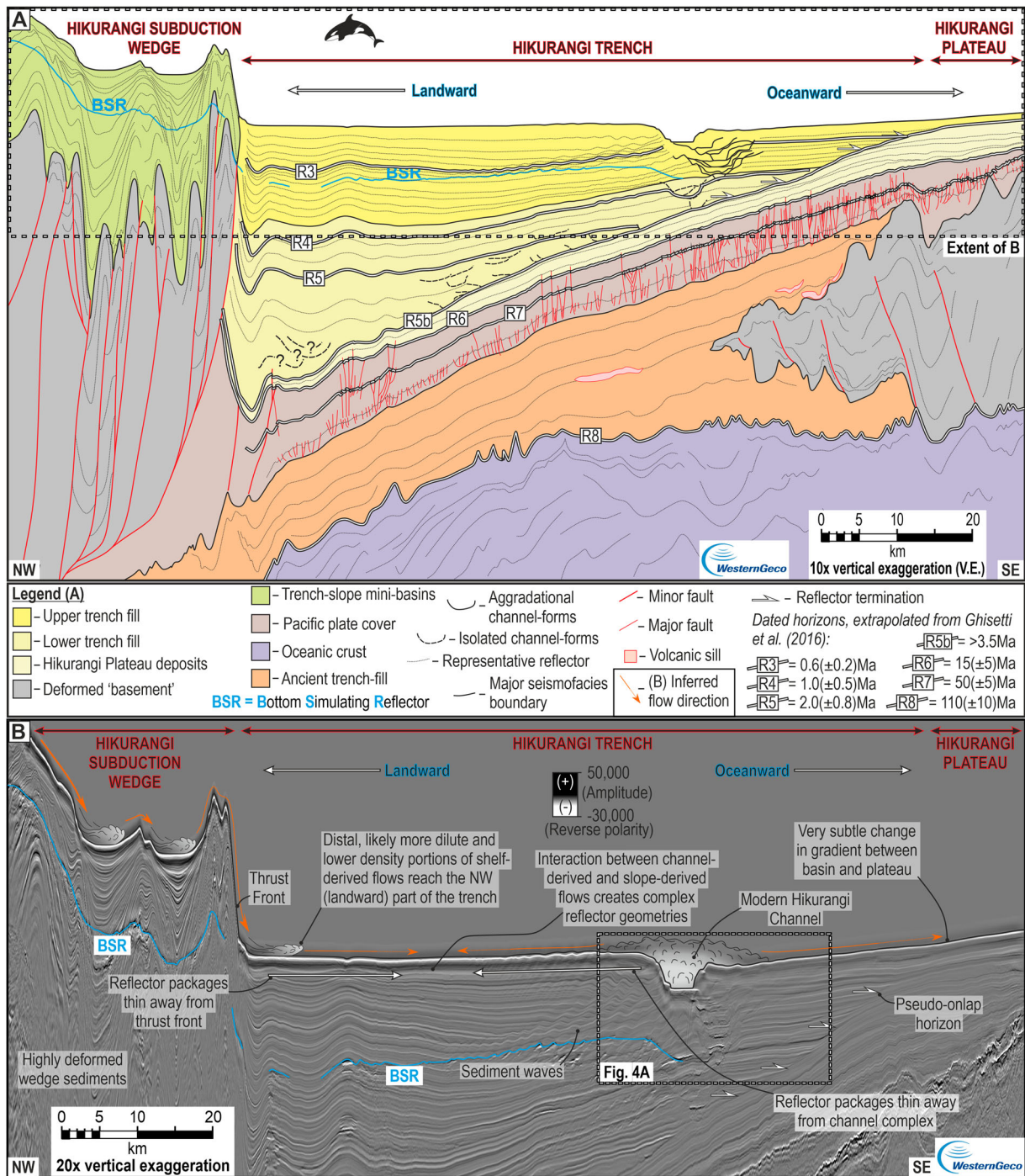


Figure 3. A, Interpreted seismic section through the Hikurangi Trench and its fill modified from McArthur and Tek (2021). **B**, Annotated part of seismic section in A, showing the key geomorphic and seismic features present in and bounding the trench-fill and the potential sources of trench sedimentation.

Methods

Bathymetry analysis and seismic interpretation

Analysis of the bathymetry and backscatter data, including the generation of depth, slope and hillshade maps, digitisation and segmentation of sediment wave crests and the channel trendline, and the generation of seafloor profiles, were conducted using ArcGISTM.

Three regionally traceable horizons (Overbank Horizons 1–3) form the basis for the subsurface interpretation. Seismic interpretation, including the

tracing of reflectors, surface generation, the mapping of sediment wave fields, and the generation of three-dimensional images was conducted in Schlumberger Petrel©. Reflectors were first traced throughout the 3D seismic volume, then extrapolated along the 2D seismic lines for the purpose of mapping the extents of the wave fields; ties between the time- and depth-domain data were conducted by identifying marker horizons present in both surveys and interpreting the position of the reflector of interest between those marker horizons. Analysis of sediment waves, which

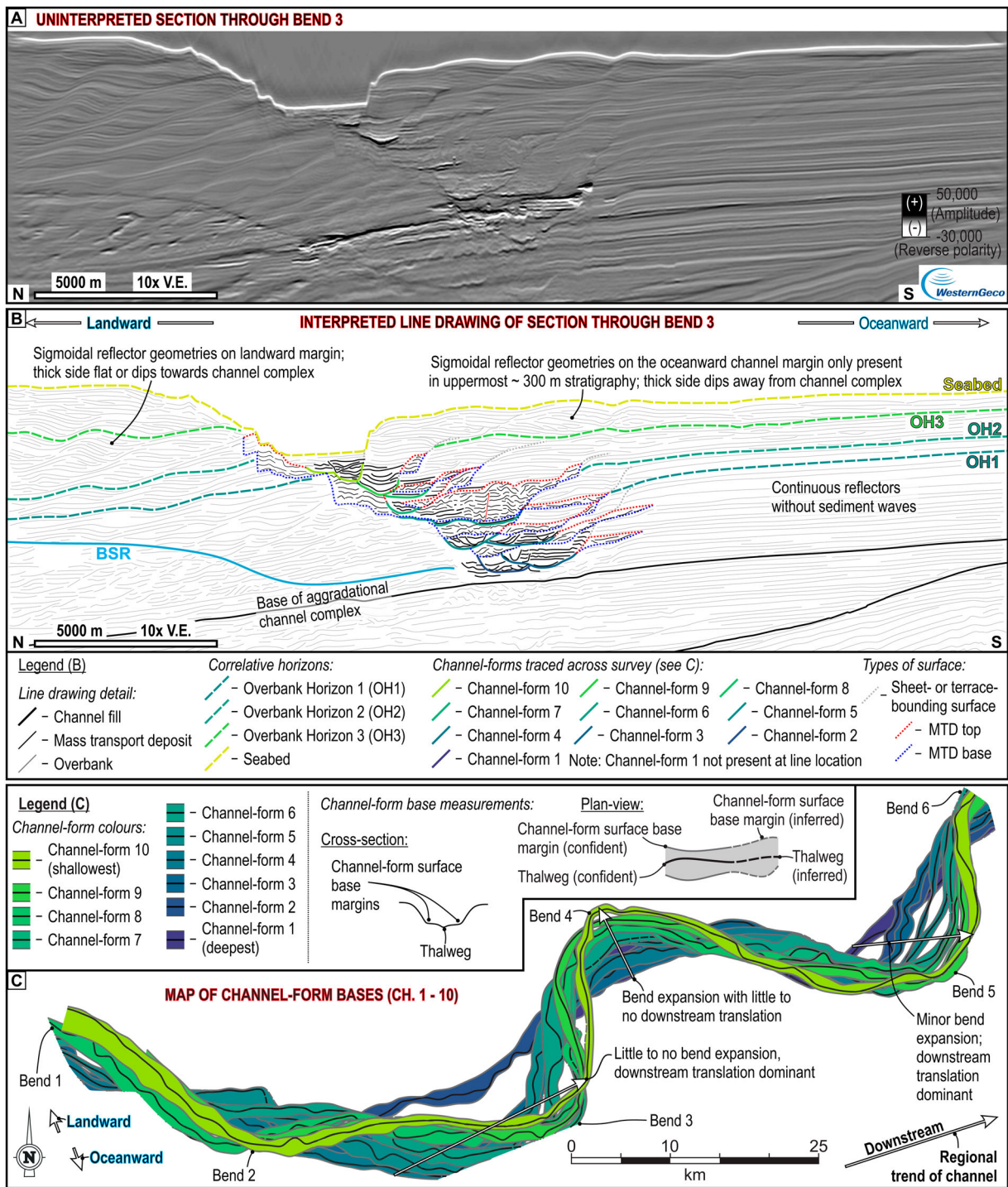


Figure 4. A, Uninterpreted seismic section (location on Figure 3B) and B, interpreted line drawing through the Hikurangi Channel and its landward and oceanward overbanks, highlighting the three subsurface horizons referenced in the text and nine of the ten channel-forms that have been traced across the study area. C, Map of the thalwegs and edges of the flat bases of the ten traced channel-forms modified from Tek et al. (2021).

was only conducted within the boundaries of the 3D survey, was achieved by importing the subsurface horizons into ArcGIS™, where they were analysed in the same way as the bathymetry data: generation of depth and slope maps, and digitisation and segmentation of wave crests.

To ensure consistency in the resolution and spatial extent of the data, and to negate the potential effect of the migration of overbank features related to the 2016

Kaikōura canyon flushing event and its associated turbidity current (Mountjoy et al. 2018), a seafloor horizon generated from the 3D seismic data is used when comparing the orientations and morphologies of overbank features in the subsurface, to those on the seafloor.

When referring to the position of waves or profiles along a channel, those in more proximal channel reaches are referred to as ‘up-channel’ when compared

to more distal, 'down-channel' reaches. Within a wave field, along an overbank transect normal to the channel, features located close to the channel are referred to as 'upstream', whereas features that are further away from a channel are referred to as 'downstream'.

Sediment wave orientations and flow analysis

The plan-view morphology of outer-bend sediment waves was used to infer modern overbank flow and palaeocurrent directions, and investigate how the orientational spread of a sediment wave field relates to the morphology of the adjacent channel (Figure 5A–C). On the seafloor, this analysis was performed on four sediment wave fields present on the landward overbank (WF1a, WF2a, WF3 and WF4; Figure 2). However, as WF2a is the only field that is imaged along its entire (up-channel to down-channel) width within the 3D seismic survey, subsurface analysis was limited to waves beneath WF2a; it should also be noted that only the upstream part of WF2a is imaged by the 3D survey.

Sediment wave crests and the trend of the adjacent channel bend were digitised and divided into 1 kilometre long segments using ArcGIS™ (Figure 5A, B); the extent of each bend is defined as the along-channel connection from the midpoint between the apex of the

relevant bend and the adjacent up-channel bend, to the midpoint between the apex of the relevant bend and the adjacent down-channel bend (Figure 5A). Channel trend segments were vectorised via connection to their down-channel neighbour, their directions were then extracted using Python programming and plotted as rose diagrams in Stereonet 10 (Cardozo and Allmendinger 2013; Figure 5B, C). The spread of segment directions is inversely proportional to the mean vector length of the orientations (Fig. 5C); hence, the inverse of mean vector length is used hereafter as a direct measure of channel bend curvature. The local overbank flow direction is assumed to be perpendicular to the local orientation of the sediment wave crests (Migeon et al. 2000; Normark et al. 2002); vectors approximating local flow direction were therefore generated at 90° to each sediment wave crest segment (directed away from the channel; Figure 5B) using Python. When local overbank flow directions are plotted on rose diagrams, the mean vector orientation indicates the mean flow direction, and the mean vector length provides an inverse measure of the bulk curvature of the sediment wave crests (Figure 5C). The relationship between channel bend, and sediment wave curvature on the seafloor and in the subsurface is examined in the 'outer-bend sediment waves' sections.

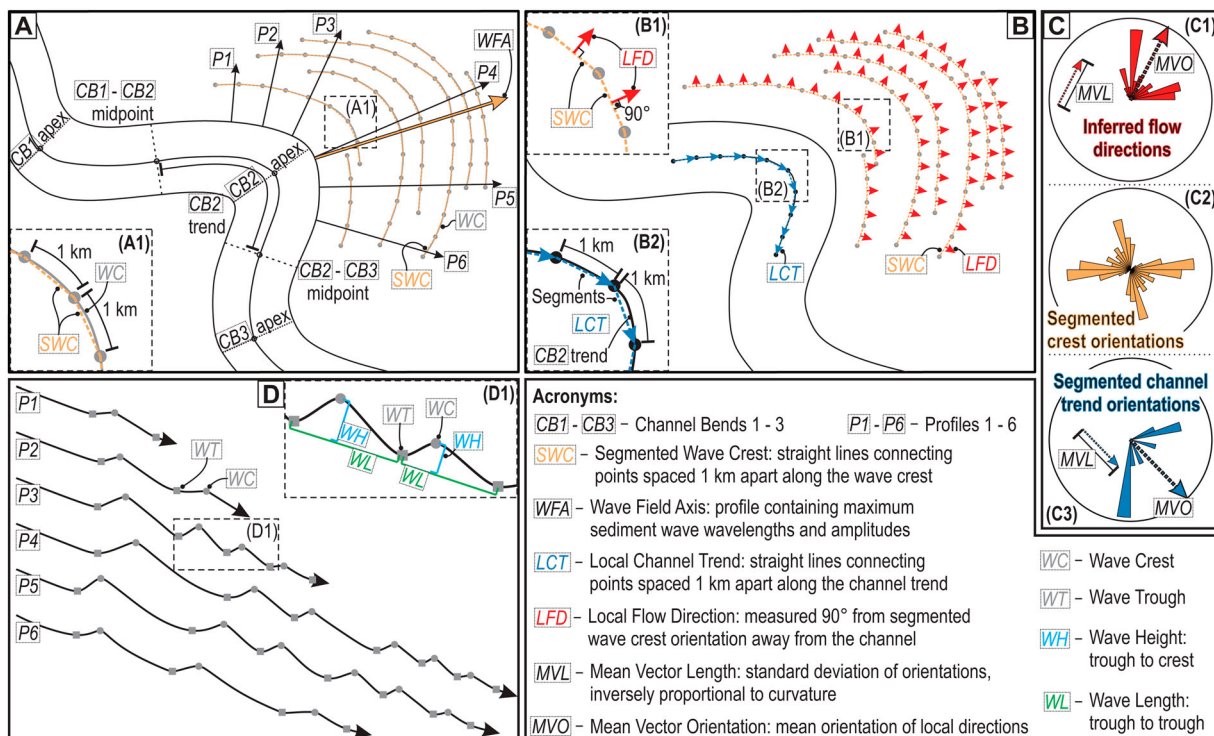


Figure 5. Schematic, fictitious example showing the methodologies applied on the seafloor and subsurface horizons for sediment wave orientations and flow analysis, and morphological analysis of the sediment waves. **A**, Shows the segmentation of the wave crests shown in **B** and **C**, the distributions of the representative longitudinal profiles used to extract wave measurements in **D**, and how channel bends are defined. **B**, Shows the segmentation of the channel bend and how inferred palaeocurrents are extracted from the segmented wave crests. **C**, Rose diagrams illustrating analysis of the orientations of overbank flow directions, of wave crests and of channel trend (data from segments in **B**). **D**, Shows how sediment wave wavelengths and wave heights are calculated in the profiles shown in **A**.

Morphological analysis of sediment waves

To analyse the size distribution of sediment waves within each outer-bend wave field and on each subsurface horizon, six longitudinal profiles, distributed incrementally along the up- to down-channel width of the field, were digitised perpendicular to the dominant wave crest orientation (Figure 5A). Along each profile, wave crests and troughs were interpreted (Figure 5D), with the interpretations validated against the plan-view expression of the identified waves. Sediment wave wavelengths are calculated as the distance between two consecutive troughs. Wave heights are calculated as the distance from a wave crest to a straight line connecting two consecutive troughs, measured normal to the trough-connecting line (Figure 5D; Ribó et al. 2016). Sediment wave dimensions and their position in their host wave field were extracted using Python™ from profiles digitised in CorelDRAW®. Wave lengths and heights are assumed to scale with increasing flow thickness (Normark et al.

2002), and hence with (unidirectional) flow velocity, meaning they can provide insight into modern flow and palaeoflow dynamics across the wave fields. A longitudinal profile through the ‘axis’ of each wave field, defined as the profile containing the largest overall wavelengths and wave heights, was also digitised but was not used in the morphometric analysis.

Results

Large-scale seafloor morphology and seismic stratigraphy

Observations

The ~250 km reach of the Hikurangi Channel in the study area exhibits steep (up to 35°) channel walls and a relatively flat channel-floor that progressively narrows from ~6.5 km in the most proximal parts, to ~1 km distally (Figures 2B and 6). In the most proximal region of the study area (Figure 2B) the channel is situated near (e.g. Bend 1; profiles 1–3, Figure 6) or at

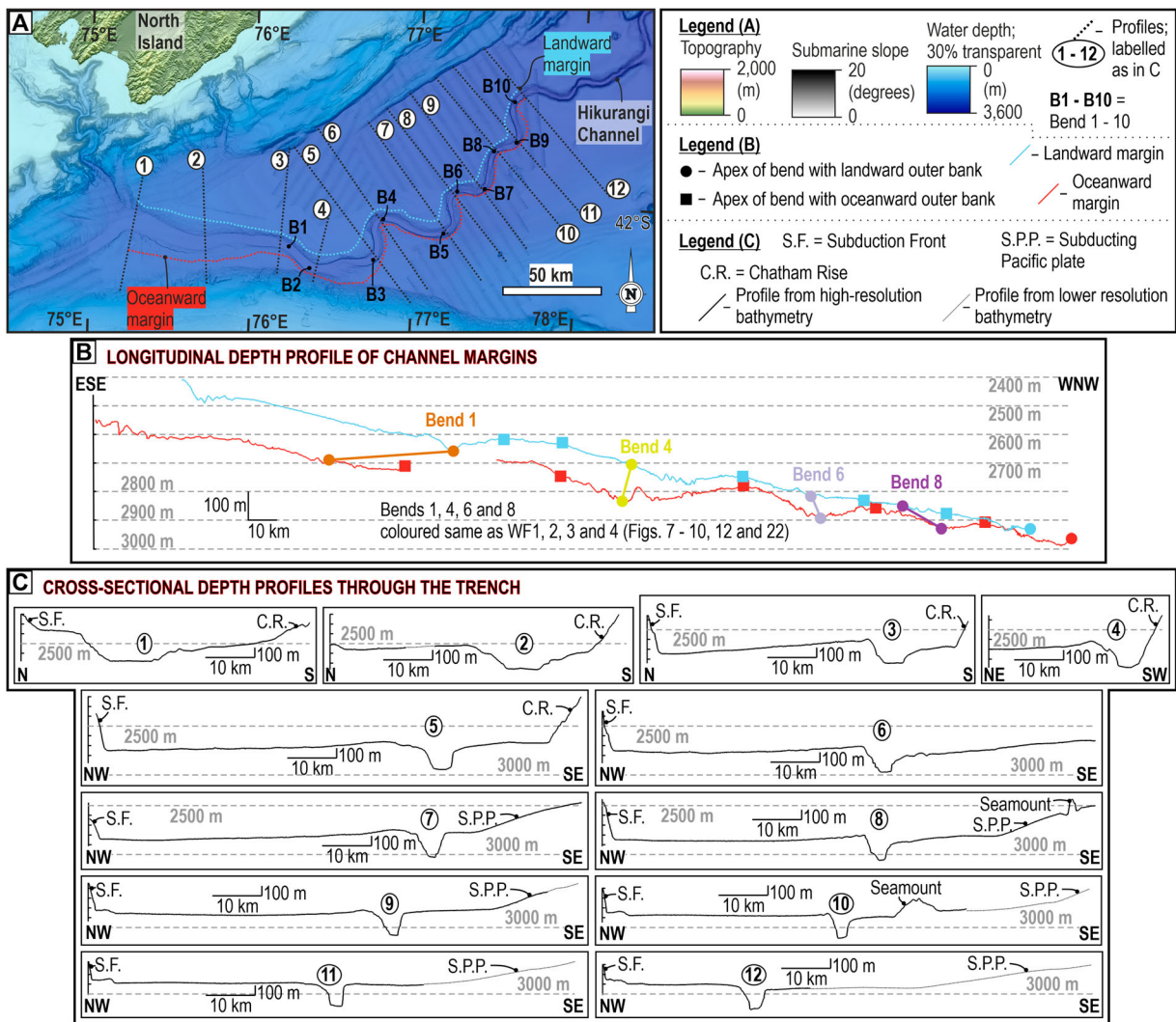


Figure 6. A, Map (location shown in Figure 2B) showing locations of the trench profiles shown in B and C. B–C, Longitudinal profiles through the trench showing the seafloor morphology of: (B) the tops of the channel walls, highlighting the depth difference between the two channel margins along the channel; (C) trench-perpendicular profiles, each through the apex of successive bends, showing the channel-perpendicular seafloor expression of the channel overbanks on both margins.

(e.g. Bend 2; profile 4, Figure 6) the northern margin of the Chatham Rise. Further down-channel, the channel is located close to the margin of the subducting Pacific plate but becomes gradually more central within the trench distally (profiles 7–12, Figure 6).

The landward (northern) channel overbank is consistently higher than the oceanward (southern) one, except where the channel is pinned against the Chatham Rise (Figure 6); the height differential is greater on bends with landward outer-bend overbanks (profiles 3, 6, 8, 10 and 12, Figure 6). The trench-floor on the landward overbank either: (a) dips gently (up to 0.8°), from a poorly defined levee crest away from the channel (NW) and toward the subduction front (e.g. profile 3, Figure 6); (b) dips gently away from the channel for tens of kilometres before becoming subhorizontal (e.g. profile 9, Figure 6); or (c) is subhorizontal across its entire width (e.g. profile 11, Figure 6). In all cases, an abrupt contact at the subduction front sees the seafloor dipping steeply (up to 35°) to the SE. The oceanward overbank either dips gently (up to 0.6°) toward the channel (NW) (e.g. profile 8, Figure 6) or is subhorizontal (e.g. profile 7, Figure 6). Where the trench-floor is bounded by the Chatham Rise, an abrupt steepening occurs at its boundary (e.g. profile 5, Figure 6); where it is bound by the subducting Pacific plate, a subtle steepening occurs (e.g. profile 9, Figure 6). In any trench-perpendicular transect in the study area, the thalweg of the channel is the deepest point of the trench (Figure 6).

At its landward edge, the trench-fill is bound by deformed subduction wedge deposits (Table 1); the contact between the two is typically marked by a frontal thrust; however, minor folding is sometimes observed in the adjacent trench-fill (Figure 3). At its oceanward edge, the trench-fill is bound proximally by the faulted strata that comprise the Chatham Rise (Table 1), and distally by strata imaged as low amplitude reflectors that top the subducting plate (Table 1). The trench-fill comprises deposits of the Hikurangi Channel, made up of channel-fill, sheet and terrace, and mass-transport deposits (Table 1; see Tek et al. 2021), and the overbank deposits studied here (Tables 1 and 2). The overbank deposits comprise most of the studied trench-fill, and can be categorised into three types (Table 2): overbank sediments with sediment waves; overbank sediments without sediment waves that terminate against the Chatham Rise or subducting plate; overbank sediments without sediment waves that terminate against the subduction front, and that display compensational wedging patterns and terminate against the subduction front.

Interpretations

The observed channel-bank asymmetry is consistent with previous studies focused on the Hikurangi Channel (Lewis et al. 1998; Lewis and Pantin 2002; Tek et al.

2021) and is interpreted to be dominantly due to leftward flow deflection by the Coriolis force. Local enhancement of overspill and aggradation on the landward margin and concomitant hindrance on the oceanward margin may be caused by flow reflection off the Chatham Rise and possibly the subducting plate, in addition to an overbank gradient that slopes towards the channel on the oceanward margin, and away from the channel on the landward margin. Elevated channel overbank heights on outer channel bends with landward outer-overbanks suggest that the centrifugal force of the flow field also enhances overspill and aggradation at these locations (Straub et al. 2008; Kane et al. 2010).

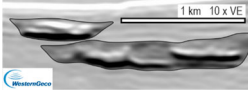
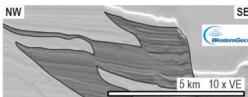
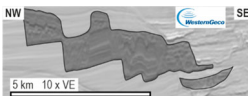
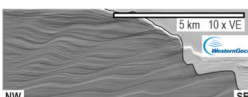
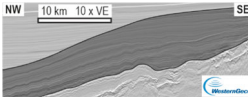
Despite the lack of well-defined levees on the seafloor, the fact that the channel-forms throughout the studied stratigraphy are bounded laterally by compound overbank deposits, with no master incision surface hosting them (Figures 3 and 4; Table 2) allows their classification as ‘aggradational’ channel deposits. The lack of a ‘wing-shaped’, tapering cross-sectional profile (a common feature of levees adjacent to aggradational channels) is due to aggradation rates being similar across the entire trench-floor. On the narrow oceanward overbank, overspilling flows can reach the edge of the trench-floor (the Chatham Rise or subducting plate) and deposit over the entire overbank area (Figure 3B). It is also possible that overbank flows may also deposit over the entirety of the wider landward overbank. Aggradation near the subduction front may be accelerated by deposition from fine-grained distal parts of flows that traversed drainage networks on the bounding slope (Figure 3B; Mountjoy et al. 2009; McArthur et al. 2019). Alternatively, overspill on the landward overbank may not reach the subduction front, with the interaction of overspilling flows and slope-traversing flows occurring somewhere in the trench.

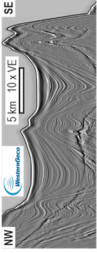
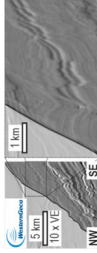
Outer-bend sediment waves on the seafloor

Observations

The four prominent sediment wave fields (WF1a, WF2a, WF3 and WF4, Figures 2B, 7 and 8) present on the landward channel overbank collectively cover 3300 km^2 of the channel overbank. Individual fields range from 130 to 1400 km^2 and extend up to 28 km away from the channel. The size (area, length and width; Figure 7) of the wave fields decreases down-channel (Figures 7D, E and 8). Waves in WF1a, WF2a, WF3 and WF4 are concentric around the outer-overbanks of bends 1, 4, 6, and 8 respectively (Figure 2C). On the seafloor, WF1a and WF2a are distinct from the wave fields present on the inner-overbanks of bends 3 and 5 (WF1b and WF2b respectively; Figure 2C). Each wave field is separate from its neighbours.

Table 1. Descriptions and interpretations of the seven seismofacies observed within and adjacent to the studied trench-fill.

Seismofacies name	Description	Amplitude	Geometry	Trench-parallel continuity	Trench-perpendicular continuity	Bound by: toward channel	Bound by: away from channel	Dip/inclination	Internal structure	Interpretation	Example
Channel-fill	Lens-shaped High-Amplitude Reflector Packages (HARPs)	High	Lens-shaped, pinch and swell over 100s – m to kms laterally, reaching < 60 m thick	10–100 s of km	<3 km	N/A; lens-shaped	Older channel-fill, sheet or terrace, MTD or overbank	Concave-up cross section; very shallow (<1°), trench-parallel dip to NE	Concave-up surfaces within packages; unilaterally migrating reflectors; transparent areas	Coarse-grained channel-fill deposits (Flood et al. 1995)	
Sheet or terrace deposits	Narrow, tabular reflector packages adjacent to channel-fills	Low – medium	Tabular	Kms – 10 s of km	Kms – 10 s of km	Channel-fill, sheet or terrace, or MTD	Sheet or terrace, MTD, or overbank	Horizontal or very gently dipping (<1°) in any direction	Sometimes gullies toward their margin away from the channel	Weakly confined, sand-rich sheet-like deposits (Pickering et al. 1995) or heterolithic terrace deposits (Babonneau et al. 2004; Hansen et al. 2015)	
Mass-Transport Deposits (MTDs)	Deformed and chaotic reflector packages	Typically low to very low; can locally contain medium or high	Highly variable: contorted reflectors or transparent	Kms – 10 s of km	Kms – ~10 km	Channel-fill, sheet or terrace, or MTD	Sheet or terrace, MTD, or overbank	Internal dips; overall dip toward channel	Folds; normal and thrust faults; and transparent zones	Mass-Transport Deposits, the product of debris flow, slumping, and sliding, comprising remobilised overbank and terrace deposits (Tek et al. 2021)	
Overbank	Laterally continuous, tabular or undulating reflector packages	Low to medium	Tabular or very subtle reflector thickening/thinning (ms over kms laterally)	10–100 s of km	10 s of km – ~100 km	Channel-fill, sheet or terrace, or MTD	Subduction front, subducting slab or Chatham Rise	Horizontal or gentle (<1°) landward (NW) dip	Sediment waves; gullies; sometimes faults	Fine grained (silt and clay), heterolithic external overbank deposits formed by overspill from channel-traversing turbidity currents (Normark et al. 1980; Pirmez and Flood 1995; Migeon et al. 2004)	
Plate-top sediments	Low amplitude, very continuous reflector packages with subtle wedging	Low	Tabular or subtle wedging in all directions (ms vertically over kms laterally)	10–100 s of km	10–100 s of km	Reflectors that terminate against trench-fill are bound by overbank; reflectors that continue under the trench, terminate against the subduction front; SE termination not imaged		Consistent landward dip < 3°, sub-parallel to dip of subducting slab	Subtle wedging; sometimes faults	Muddy hemi-pelagites and contourites deposited on the pacific plate during subduction (Barnes et al. 2020)	

Subduction wedge deposits	Heavily folded reflector packages with variable thicknesses	Low to high; increases toward seabed	Highly variable in reflector thickness (ms vertically over kms laterally) and amplitude over metres to kms	Kms – 10 s of km	Kms – 10 s of km	Overbank	N/A; outside of study area	Highly variable dips due to structure; flat to sub-vertical and locally overturned reflectors	Thrust-cored anticlines, fanning reflectors, axis-thickening synforms	Coarse-grained deposits of trench slope mini-basins and the structures that bound them (McArthur et al. 2019)	
Chatham Rise deposits	Heavily faulted reflector packages with internal truncations	Low to high	Packages and reflectors traceable over 10s to 100s of km, subtly thinning toward subduction front; reflector displacement/abrupt dip changes common	10–100 s of km	10–100 s of km	Trench-fill of any type: channel-fill, sheet or terrace, MTD, or overbank	N/A; outside of study area	Packages follow dip of subducting plate, < 3° NW; dips of reflectors vary abruptly at faults	Pervasive normal faults (10s to 100s of m offset), spaced 100 m – 5 km apart	Sedimentary rocks that comprise the upper part of the Chatham Rise (Davy et al. 2008)	

Bend 4 exhibits the greatest curvature (lowest mean vector length), followed by bends 6 and 8; bend 1 is the straightest (Figure 8). The down-channel limit of WF2a and WF3 is further down-channel of the apex of their associated bends than the up-channel limits of the wave fields; WF1a and WF3 are more symmetric about the apex of their associated bends (Figures 7 and 8). The orientations of the segmented wave crests, and therefore the inferred local flow directions, exhibit the greatest spread (inversely proportional to mean vector length) in WF2a, and the least in WF1a (Figures 8, 9A and C). Except on WF4, the ‘axis’ of the wave field (the channel-perpendicular transect containing the largest waves; Figure 5) is consistently orientated down-channel of the mean flow direction (mean vector orientation; Figures 8 and 9A).

In crest-perpendicular transects (see profiles 1–6; Figure 8), sediment waves typically have narrow stoss sides that can be horizontal, or dip gently toward the channel, and wider lee sides that dip more steeply away from the channel (Figure 10). Stoss sides exhibit higher backscatter reflectivity and Root Mean Squared (RMS) amplitude values than lee sides (Figure 11A, B).

Waves on the seafloor exhibit wavelengths that range from 6639 to 439 m with a mean wavelength of 1734 m (Figure 12; Tables 3 and 4). Wave heights range from 48 m to below the data resolution (<1.5 m) with a mean height of 9 m (Figure 12; Tables 3 and 4); smaller waves are likely present but undetectable at the resolution of the available data (Figures 10 and 12A). No systematic wavelength or wave height trends are observed between successive bends moving down-channel (Figure 12A); however, the maximum wavelength and height in each wave field does decrease down-channel (Table 3). Most profiles (Figure 8) display a systematic downstream decrease in wave height (Figures 10 and 12B). In some profiles individual wavelengths and the overall range of wavelengths also decrease downstream (e.g. WF1a axis; Figures 10 and 12B); however, a systematic downstream variation in wavelength is not apparent (Figure 12B). Wavelengths and wave heights decrease toward the up-channel and down-channel margins of each wave field, and therefore away from the bend apex (Figures 8, 10 and 12C). The decrease in wavelength and height is more abrupt at the down-channel margin of the field. The profiles containing the highest maximum and average wavelengths and heights (profiles 3, 4 or 5) are located toward the middle of each sediment wave field (Figure 12C).

Interpretations

The exclusive presence of outer-bend wave fields on only the landward margin suggests that the velocity and/or magnitude of the overspilling flow was enhanced on the landward and hindered on the oceanward overbank. This may have occurred due to: (a) the

Table 2. Descriptions, interpretations, and seismic cross-sections of the three types of overbank geometry observed within the studied trench-fill.

Overbank type	Description	Occurrence/context	Interpretation
	<p>Overbank sediments with sediment waves</p> <p>Laterally continuous low to medium amplitude reflectors that systematically thicken and thin to form sigmoidal sediment waves. While some individual reflectors may disappear in the thin limb of the sediment waves, most reflectors can be traced across the length of the wave field.</p>	<p>Present through shallowest ~700 m of stratigraphy. Dominantly observed on the landward channel margin. Toward the channel, reflectors terminate abruptly against channel-fill, terrace deposits, or MTDs (Table 1). Away from the channel, reflectors transition into overbank sediments without sediment waves that terminate against the subduction front.</p>	<p>Fine grained overbank sediment waves formed by unidirectional overspilling flow from turbidity currents that traversed the Hikurangi Channel and its palaeo-incarnations. Aggradation occurs faster on their upstream (toward the channel) limb and they migrate toward the channel.</p>
	<p>Overbank sediments without sediment waves that terminate against Chatham Rise/subducting plate</p> <p>Reflectors are tabular or subtly thin away from channel. On the side away from the channel, reflectors thin and either terminate or steepen abruptly against subducting plate-top sediments.</p>	<p>This overbank type is only observed on the oceanward (SE) channel margin. The contact between overbank reflectors and plate-top sediments (Table 1) migrates vertically and oceanward through the stratigraphy.</p>	<p>'Confined external levee' sensu Clark and Cartwright (2011) deposited by overspilling flow from turbidity currents that deposited over the entire area between the channel and the oceanward trench margin (bound by the Chatham Rise or top of the subducting plate).</p>
	<p>Overbank sediments without sediment waves that terminate against the subduction front</p> <p>Reflectors are generally laterally continuous and usually thicken away from the channel (example 1 above). However, reflectors and reflector packages thin and occasionally pinch out onto highs and thicken into lows exhibited by deeper reflectors (example 2 above). In both cases, reflectors are deformed near to, and abruptly terminate against, the subduction front.</p>	<p>This overbank type is only observed on the landward (NW) channel margin. The expression of deep structures, typically thrust-cored anticlines, is muted toward the seafloor, which is generally subhorizontal. Structures are more common nearer the subduction front, sometimes causing packages of overbank reflectors to thin away from the channel.</p>	<p>These deposits likely represent a combination of fine-grained deposition from overspilling flow from the Hikurangi Channel, and the fine-grained, dilute, distal expression of flows that traverse the trench-slope basins of the Hikurangi Subduction wedge. Sediments from both sources collectively act to heal the expression of growing structures and maintain a relatively flat seafloor.</p>

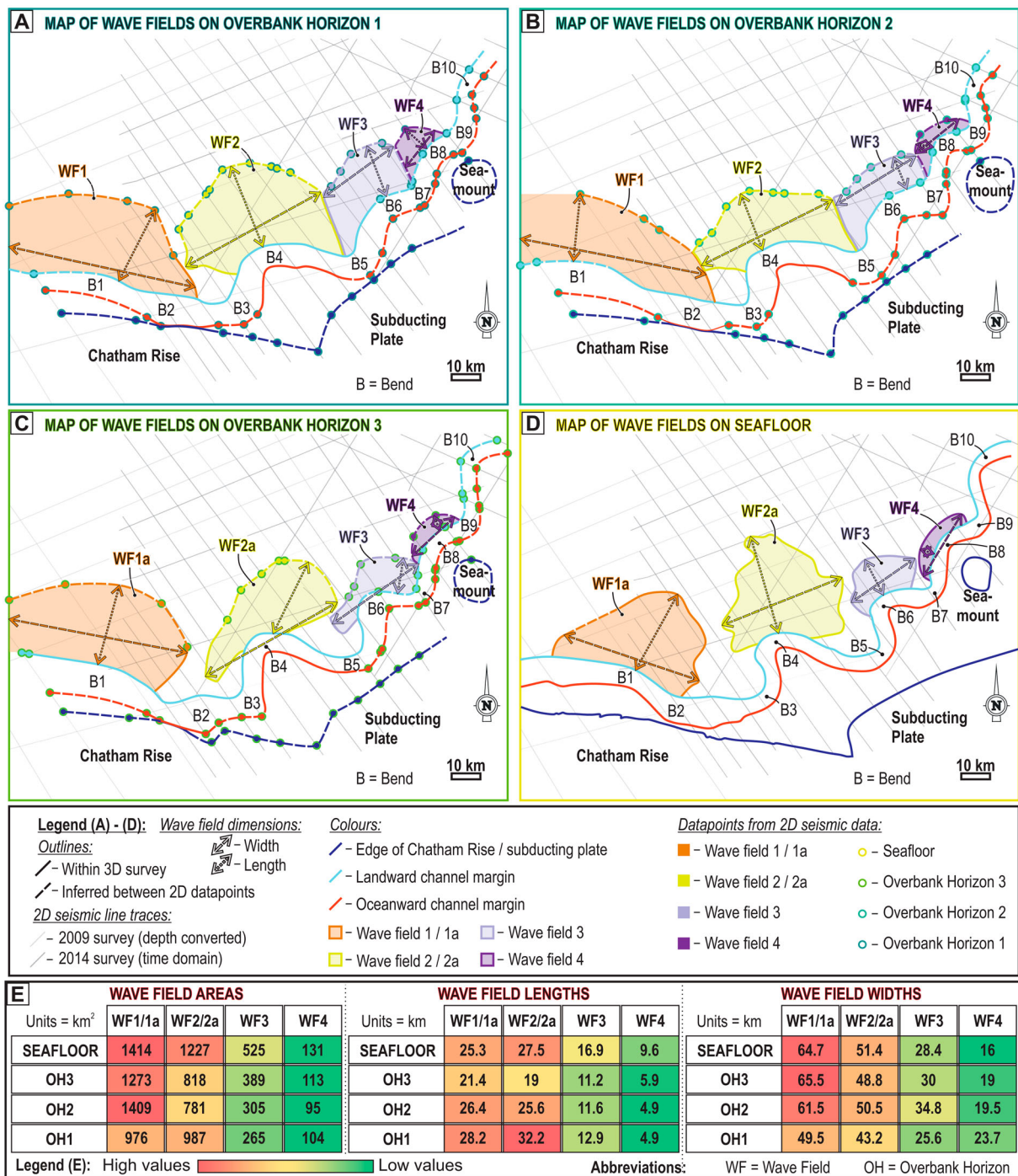


Figure 7. A–D, Topological maps of the four outer-bend wave fields on the landward channel margin, highlighting their stratigraphic evolution from Overbank Horizon 1 (A), through Overbank Horizons 2 (B) and 3 (C), to the seafloor (D). **E,** Dimensions of the wave fields in A–D, showing area, length (measured away from the channel), and width (measured along the channel).

influence of the Coriolis force (Wells and Cossu 2013), or (b) overspilling flow reflecting (Kneller et al. 1991; Bell et al. 2018) off the Chatham Rise and/or the subducting plate generating a transverse (landward; to the northwest) component of flow that likely counteracts overspill on the oceanward margin, and potentially aids overspill on the landward margin. scenario (a) likely affects the whole channel, whereas the effects of (b) are likely to be spatially variable. The observed down-channel decrease in wave field size is potentially a result of flow tuning, whereby the portion of a flow

capable of overspilling systematically decreases down-channel as the flow thins due to material being lost from the upper part of the flow as it traversed successive up-channel bends (Mohrig and Buttles 2007; Kelly et al. 2019). However, the East Cape Current, a contour current that flows SW along the subduction front before turning anti-clockwise and crossing the channel in the location of the study area (Fernandez et al. 2018), may counteract overbank flow on the landward margin in the distal parts of the study area, further inhibiting sediment wave development in WF3 and WF4.

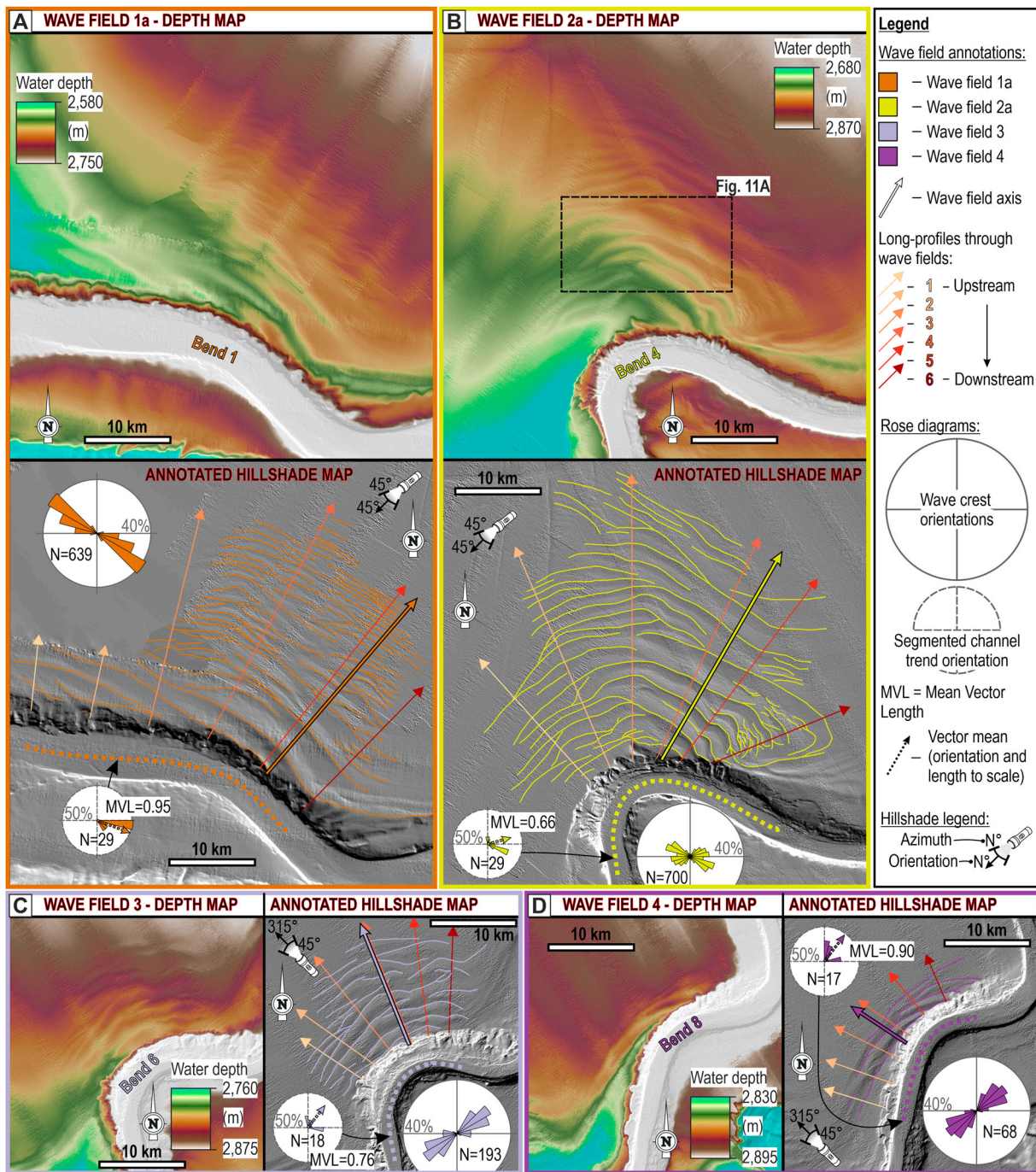


Figure 8. Maps showing **A**, the seafloor expression of wave field 1a, **B**, wave field 2a, **C**, wave field 3, and **D**, wave field 4. For each wave field, an uninterpreted depth map and an interpreted hillshade map are displayed. On the interpreted map, the wave crests, the trend of the related channel bend, the locations of the longitudinal profiles shown in Figure 10, including the wave field axis, and two inset rose diagrams showing the (bi-directional) orientations of the wave crest segments and the vector directions of the segmented channel bend trend are highlighted.

The observed pattern of diminishing wave heights up- and down-channel from the wave field axis is interpreted as the result of overbank flow travelling sub-perpendicular to the wall of the channel bend it originates from, which typically occurs along most of the length of that bend. Thus, bulk wave curvature in a wave field generally scales proportionally with the curvature of its formative bend (Figure 9C). However, the action of centrifugal force leads to increased overspill, and consequently the generation of larger

waves, downstream of the bend apex, with overspill diminishing up- and down-channel from the wave field axis (Straub et al. 2008).

The wavelengths and heights of the outer-bend waves observed here are consistent with the ranges quoted by Wynn and Stow (2002) for those on levees (<7 km and <80 m respectively). Cores from the overbanks of the Hikurangi Channel examined by Lewis and Pantin (2002) and Mountjoy et al. (2018) contain thin-bedded turbidites that grade from fine sand or silt

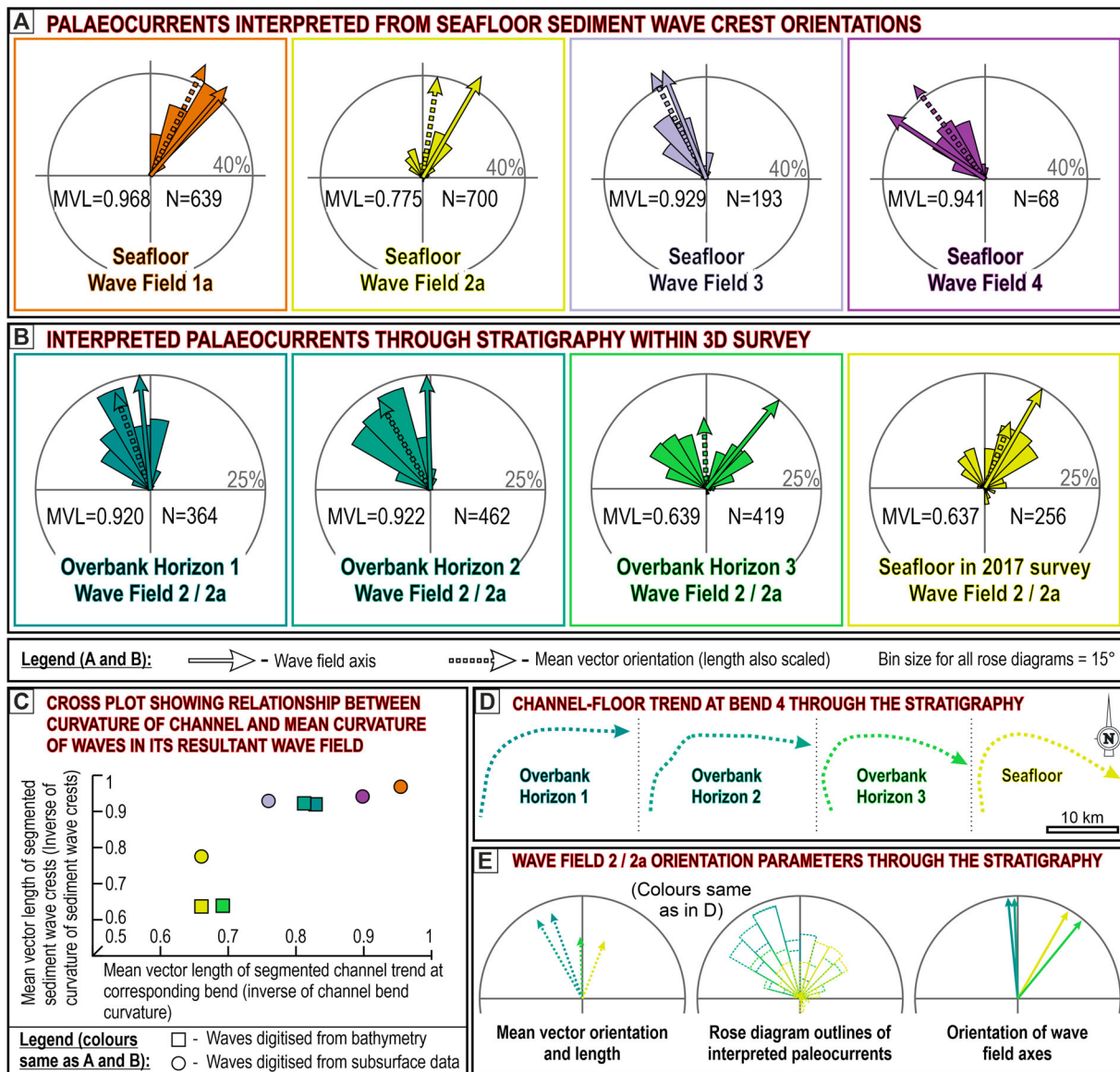


Figure 9. **A**, Rose diagrams showing the orientations of interpreted palaeocurrents from wave fields 1a, 2a, 3 and 4 on the seafloor, calculated from the segmented wave crests. **B**, Rose diagrams showing the orientations of interpreted palaeocurrents from wave field 2/2a in the 3D seismic survey Overbank Horizon 1, 2, 3 and the seafloor. **C**, Graph showing the relationship between the bend curvature, and the bulk curvature of the wave crests in their associated wave fields, calculated using the mean vector lengths of the segmented channel trend and the interpreted palaeocurrents from the segmented wave crests. **D**, Plan-view of the trend of bend 4 through the stratigraphy, showing an overall increase in bend curvature from Overbank Horizon 1 to the seafloor. **E**, Hemispheric rose diagrams showing the mean vector orientation and length, interpreted palaeocurrents, and orientation of wave field axis through the stratigraphy, showing an overall clockwise rotation from the deep stratigraphy (Overbank Horizons 1 and 2), to the shallow stratigraphy (Overbank Horizon 3) and the seafloor.

to mud (a mixture of silt and clay), which is also consistent with typical grain-sizes observed on submarine channel overbanks (Wynn and Stow 2002). High backscatter and RMS amplitude values observed on the stoss sides of the waves (Figure 11A and B) suggest that the stoss sides of the sediment waves contain coarser sediment than the lee sides; this finding is consistent with observations made by Lewis and Pantin (2002). These patterns may arise due to coarse-grained sediment being preferentially bypassed on the lee sides where finer-grained deposits form from the tails of overspilling flows. Meanwhile, on the upstream-

dipping stoss sides deposition of a wider grain-size range is permitted.

Outer-bend sediment waves in the subsurface

Observations

In the subsurface, waves are present through the shallowest 800 m of stratigraphy, although only the upper 600 m of stratigraphy is the focus of this study. In crest-perpendicular cross-sections, they exhibit sigmoidal geometries with thicker reflectors on their stoss sides, and their troughs and crests consistently

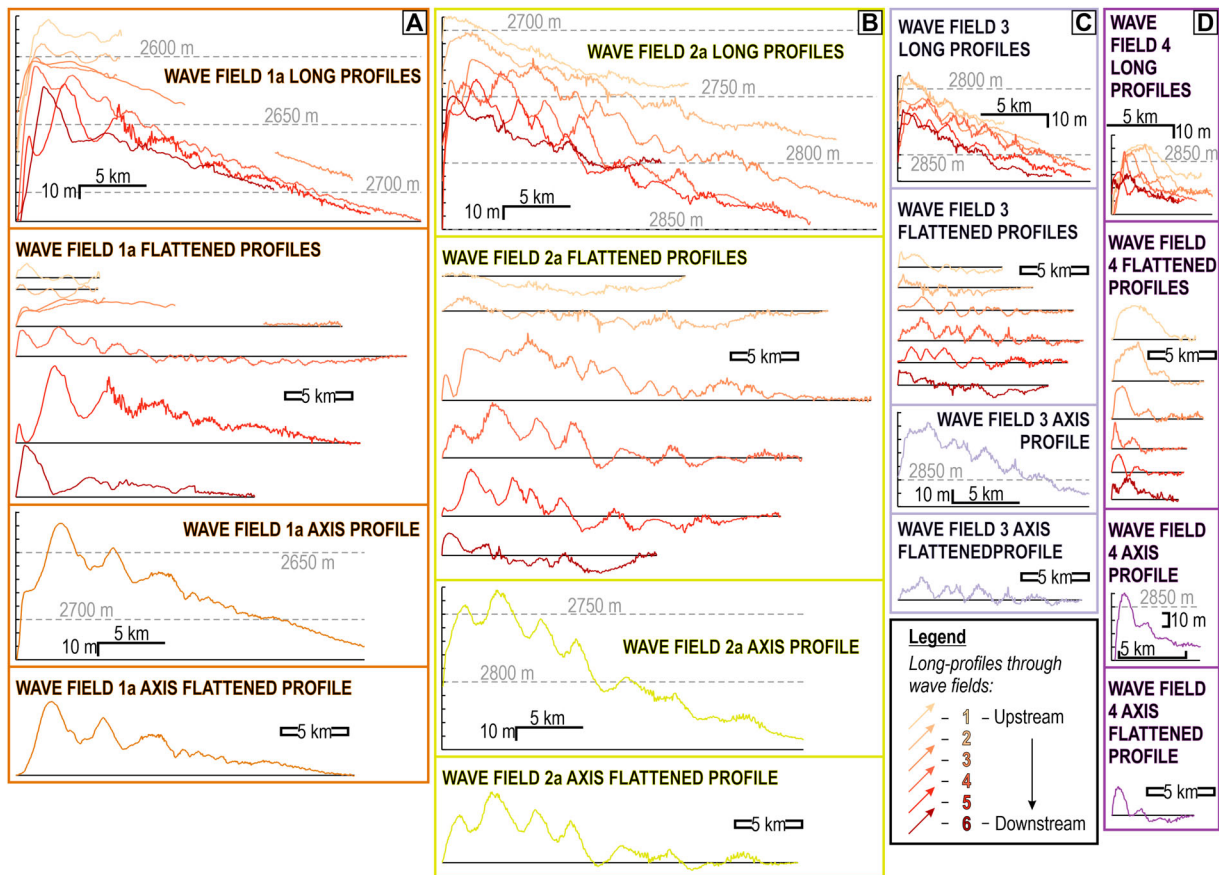


Figure 10. Crest-perpendicular seafloor profiles (locations shown in Figure 8) through wave fields 1a (A), wave field 2a (B), wave field 3 (C), and wave field 4 (D). For each wave field, the six profiles used for the extraction of wave dimensions in Figure 12 are shown in depth and flattened to their upstream and downstream ends, and the wave field axis (profile containing the largest overall wavelength and wave heights), which is also shown in depth and flattened.

stack toward the channel (Figure 11C). Reflectors also exhibit higher RMS amplitudes on their stoss sides than their lee sides (Figure 11B). The same four outer-bend wave fields observed on the seafloor have been mapped in the subsurface (WF1/1a, WF2/2a, WF3 and WF4; Figure 7) on three subsurface horizons (Overbank Horizons 1–3; shallowing respectively; Figures 4 and 7). A down-channel decrease in wave field size is observed on all subsurface horizons (Figure 7). The fields appear to show a general upward increase in area through the stratigraphy (Figure 7E), but this may be due to diminished data resolution at depth impeding detection of smaller waves at the extremities of the field. The wave fields also change shape through the stratigraphy, from being relatively wide (along-channel) and short (distance away from the channel) fields that interfinger with their up-channel and down-channel neighbours in the deeper stratigraphy (Figure 7A, B), to being narrow and long seafloor wave fields that are distinct from their neighbours (Figure 7D).

Analysing the 3D distributions and morphologies of waves through the stratigraphy beneath WF2a permits an examination of the evolution of the wave field. The curvature of bend 4 (the formative bend of WF2a) increases through progressively shallower stratigraphy

(Figures 9D and 13), accompanied by: (a) an increase in the spread of the wave crest segment orientations and inferred palaeoflow (Figures 9B, C and 13), (b) a down-channel shift and rotation of the up-channel and down-channel extent of the wave field, the mean palaeoflow orientation (mean vector orientation of palaeocurrents), and the wave field axis (Figures 9B, E and 13). The axis of WF2/2a is consistently positioned down-channel of the mean palaeocurrent orientation and the apex of bend 4 (Figure 9B).

The wave heights and wavelengths (Tables 3 and 4) in WF2/2a become larger through progressively shallower stratigraphy but appear to be smaller on the seafloor than in Overbank Horizon 3 (Figures 12A, 13 and 14). Similar trends of wave morphology to those observed on the seafloor are observed throughout the subsurface: crest-perpendicular transects typically display a downstream decrease in wave height (Figures 12B, 13 and 14), and wave heights and wavelengths generally increase toward the centre of the wave field (Figures 12C, 13 and 14).

Interpretations

The cross-sectional geometries of the waves are consistent with upstream-migrating sediment waves observed on the overbanks of many other submarine

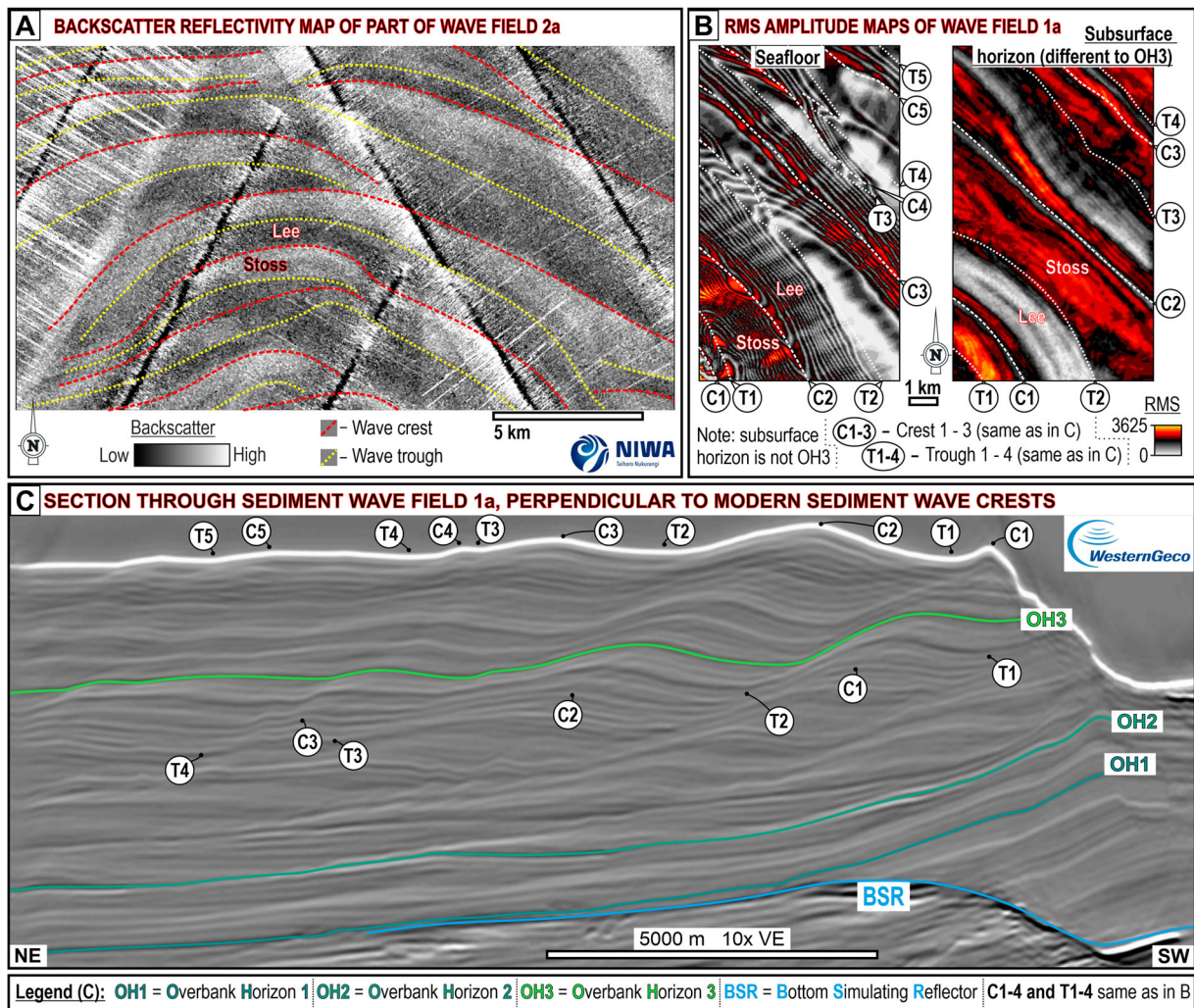


Figure 11. **A**, Seafloor backscatter map imaging part of wave field 2a, showing that higher backscatter values occur on the upstream stoss sides of waves than on their lee sides. **B**, Root Mean Squared (RMS) amplitude maps from the seafloor and the subsurface (depth shown in C) showing that, in general, RMS values are higher on the stoss (SW) sides of the waves in wave field 1. **C**, Crest-perpendicular seismic section through wave field 1a, showing the locations of the three subsurface horizons and the locations of the horizons in **B**.

channel systems, wherein deposition on the shallow or upstream-dipping stoss sides occurs faster than on the lee sides, where bypass prevails (e.g. Migeon et al. 2000, 2001; Nakajima and Satoh 2001; Normark et al. 2002). Observed reflector thickness trends (thicker stoss sides) and RMS amplitude trends (higher on the stoss sides) can be generated by either the 'lee wave' (Flood 1988; Lewis and Pantin 2002) or 'cyclic-step' (Slootman and Cartigny 2020) models (Figure 1).

At the time of Overbank Horizons 1 and 2, the channel was straighter compared to the modern channel and likely had steeper outer-levee gradients, allowing almost continuous overspill on the landward overbank, with a slight superimposed increase in overspill toward bend apices. Coriolis forcing likely enhanced overspill on the landward overbank. Through time, as the channel became more sinuous, centrifugal force became more dominant causing a

focusing of thicker, faster overbank flow just downstream of the bend apices (Hay 1987; Straub et al. 2011), leading to: (a) a separation of the wave fields from their up-channel and down-channel neighbours, (b) an increase in wave crest curvature, and (c) a down-channel shift in the wave field axis, the mean inferred flow orientation, and the up-channel, and down-channel limits of the wave fields. Effects of bend expansion may have been enhanced by diminishing outer levee gradients as trench sedimentation from transverse drainage networks became more voluminous and suppressed levee growth (see 'large scale trends' section above).

Up-stratigraphy increases in average wave heights and wavelengths (Figure 12A) may reflect an enhancement in maximum overspilling flow velocities within each wave field due to increasing centrifugal influence, or combination of compactional effects and limits in data resolution; however, temporal variability in the

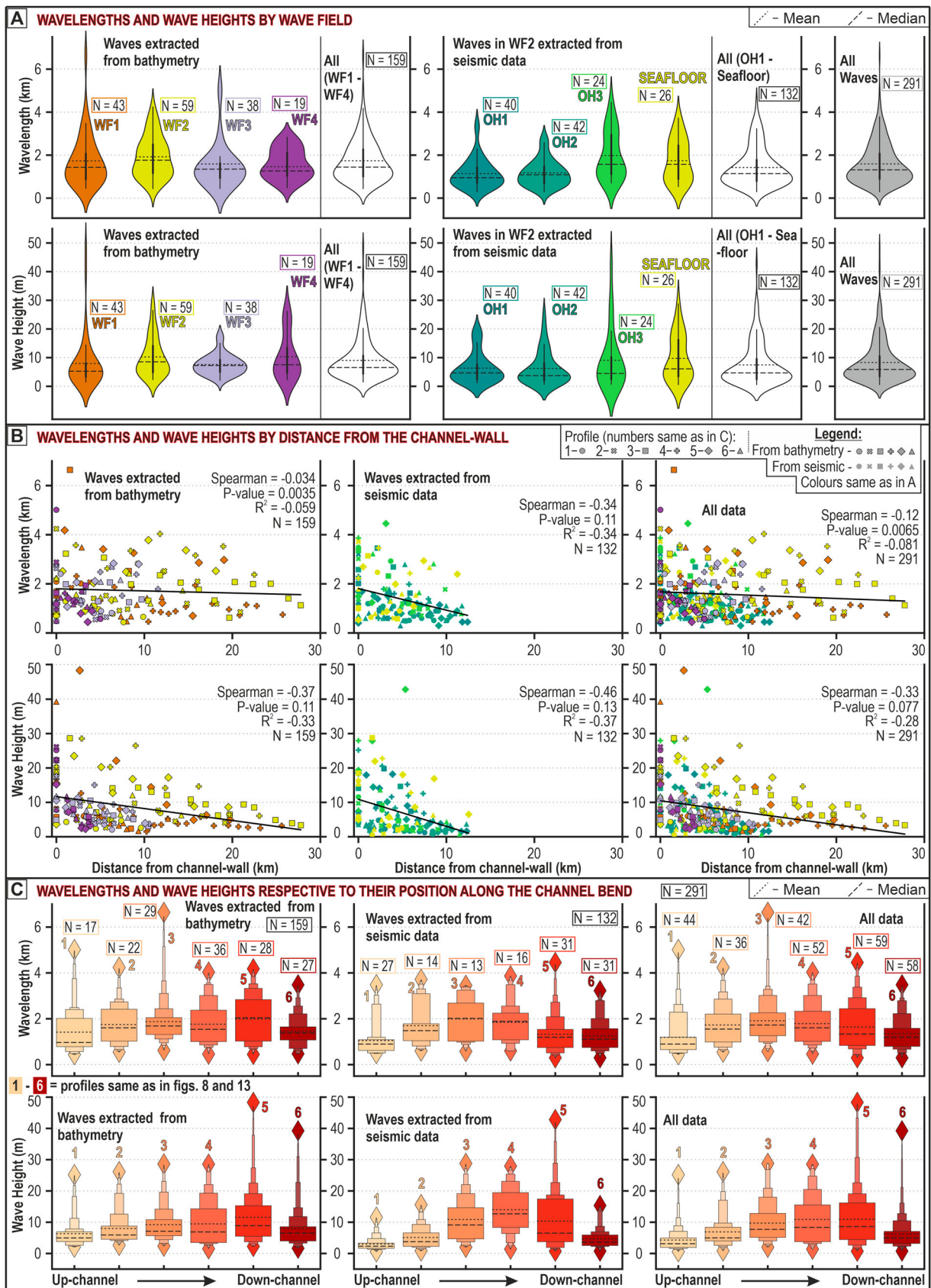


Figure 12. A, Violin plots showing the distributions of sediment wave wavelengths and wave heights displayed by wave field on the seafloor and by measured Overbank Horizon in the subsurface for waves in wave field 2. B, Scatterplots showing wavelengths and wave heights extracted from bathymetry data (coloured by wave field), seismic data from wave field 2 (coloured by the horizon they were extracted from), and all data. Separate plots of wave height versus distance from channel wall for each wave field and profile are provided as supplementary material. C, Letter-value plots (Hofmann et al. 2017) showing wavelengths and wave heights displayed by profile number (profiles 1–6 in Figures 8 and 10) highlighting up- to down-channel variability in the morphology of waves extracted from bathymetry, seismic, and all data; diamonds represent the minimum (resolvable) and maximum values, and boxes are scaled proportionally to number of datapoints.

Table 3. Minimum (resolvable), maximum and average wavelengths and heights of the sediment waves in each wave field.

	Name	Wavelength (m)				Wave Height (m)				No. of readings (N)
		Minimum	Maximum	Mean	Median	Minimum	Maximum	Mean	Median	
Measured From Bathymetry	Wave Field 1	460	6639	1730	1430	1.5	48.3	8.0	5.2	43
	Wave Field 2	439	4240	1919	1763	2.3	28.6	10.3	8.5	59
	Wave Field 3	484	2829	1589	1352	2.1	17.7	7.6	7.3	38
	Wave Field 4	447	5013	1461	1266	2.3	26.1	10.3	7.5	19
Measured From Seismic	All From Bathymetry	439	6639	1734	1439	1.5	48.3	9.0	6.6	159
	Overbank Horizon 1, Wave Field 2	299	3454	1142	949	1.2	19.8	6.3	4.7	40
	Overbank Horizon 2, Wave Field 2	299	2793	1172	1088	0.7	25.2	6.2	3.7	42
	Overbank Horizon 3, Wave Field 2	705	4455	1981	1571	0.7	42.8	9.0	4.5	24
	Seafloor, Wave Field 2	534	3718	1739	1571	0.6	28.8	9.8	6.1	26
	All From Seismic	299	4455	1422	1142	0.6	42.8	7.5	4.7	132
All Data		299	6639	1592	1314	0.6	48.3	8.3	5.9	291

Table 4. Minimum (resolvable), maximum and average wavelengths and heights of sediment waves across all fields, displayed by profile (shown in Figures 8 and 13); profile 1 is furthest up-channel and profile 6 is furthest down-channel.

	Name	Wavelength				Wave Height				No. of readings (N)
		Minimum	Maximum	Mean	Median	Minimum	Maximum	Mean	Median	
Measured From Bathymetry	Profile 1	439	5013	1416	968	2.1	25.2	6.3	5.0	17
	Profile 2	546	4240	1747	1604	2.6	26.1	8.0	5.9	22
	Profile 3	622	6639	1878	1687	2.4	28.6	9.2	7.1	29
	Profile 4	460	4033	1764	1540	1.5	28.5	9.5	6.9	36
	Profile 5	447	4179	1993	2044	2.3	48.3	11.6	8.9	28
	Profile 6	473	3483	1462	1383	1.7	39.2	8.0	6.5	27
Measured From Seismic	Profile 1	490	3483	1049	896	0.6	11.6	3.0	2.3	27
	Profile 2	598	3718	1700	1482	0.8	15.6	5.1	3.8	14
	Profile 3	577	3454	1995	2016	2.0	28.8	10.9	9.1	13
	Profile 4	597	3868	1844	1887	1.4	28.0	14.0	12.7	16
	Profile 5	299	4455	1328	1194	0.7	42.8	10.4	6.5	31
	Profile 6	299	3227	1255	1109	0.7	15.3	4.7	3.6	31
All Waves	Profile 1	439	5013	1191	896	0.6	25.2	4.3	3.1	44
	Profile 2	546	4240	1729	1550	0.8	26.1	6.9	5.0	36
	Profile 3	577	6639	1914	1725	2.0	28.8	9.7	7.7	42
	Profile 4	460	4033	1789	1606	1.4	28.5	10.9	8.4	52
	Profile 5	299	4455	1644	1337	0.7	48.3	10.9	8.6	59
	Profile 6	299	3483	1351	1196	0.7	39.2	6.2	5.0	58

average thickness of channel-traversing flows related to changes in sediment supply entering the system from the feeder canyons cannot be discounted.

Inner-bend overbank waves on landward channel margin

Observations

On the seafloor discrete wave fields are observed on the inner-overbanks of bends 3 and 5 (WF1b and WF2b; Figure 2C); these are smaller (~105 and ~115 km² respectively) than adjacent outer-bend fields and are not present in the deepest studied stratigraphy (Overbank Horizons 1 and 2). On Overbank Horizons 1 and 2, the down-channel ends of waves in WF2 interfinger with the up-channel ends of waves in WF3. Between Overbank Horizon 2 and 3, WF2 divides into two distinct fields (Figure 15): 'WF2a', within which waves are arcuate and broadly concentric around the outside of bend 4 (Figure 13), and 'WF2b', where waves are relatively straight and orientated at a high angle to the channel-wall (WSW-ENE) (Figure 15D). WF1 shows

a similar division into WF1a and WF1b. Wave crests at the down-channel end of WF2a are orientated sub-perpendicular to the crests of waves in WF2b, and terminate abruptly along a boundary that follows the crests of the waves in WF2b. In Overbank Horizon 3, waves in WF2b interfinger with waves in WF3, but on the seafloor WF2b and WF3 are distinct (Figures 13 and 15).

Waves in WF2b (visible on Overbank Horizon 3 and the seafloor) exhibit wavelengths of < 1500 m (mean 1250) and heights of < 20 m (mean 10) at their up-channel (WSW) end. Wavelengths and heights decrease downstream and down-channel (Figure 15), where they branch into multiple smaller waves that interfinger with waves in WF3 (e.g. on Overbank Horizon 3; Figure 15C) or diminish to heights below data resolution (e.g. on the seafloor; Figure 15D). On the seafloor, immediately NE of WF2a, is a broad, flat area devoid of sediment waves (Figure 15D) that sits stratigraphically above buried waves. This area constituted the upstream part of WF3 in Overbank Horizon 3 (Figure 15C).

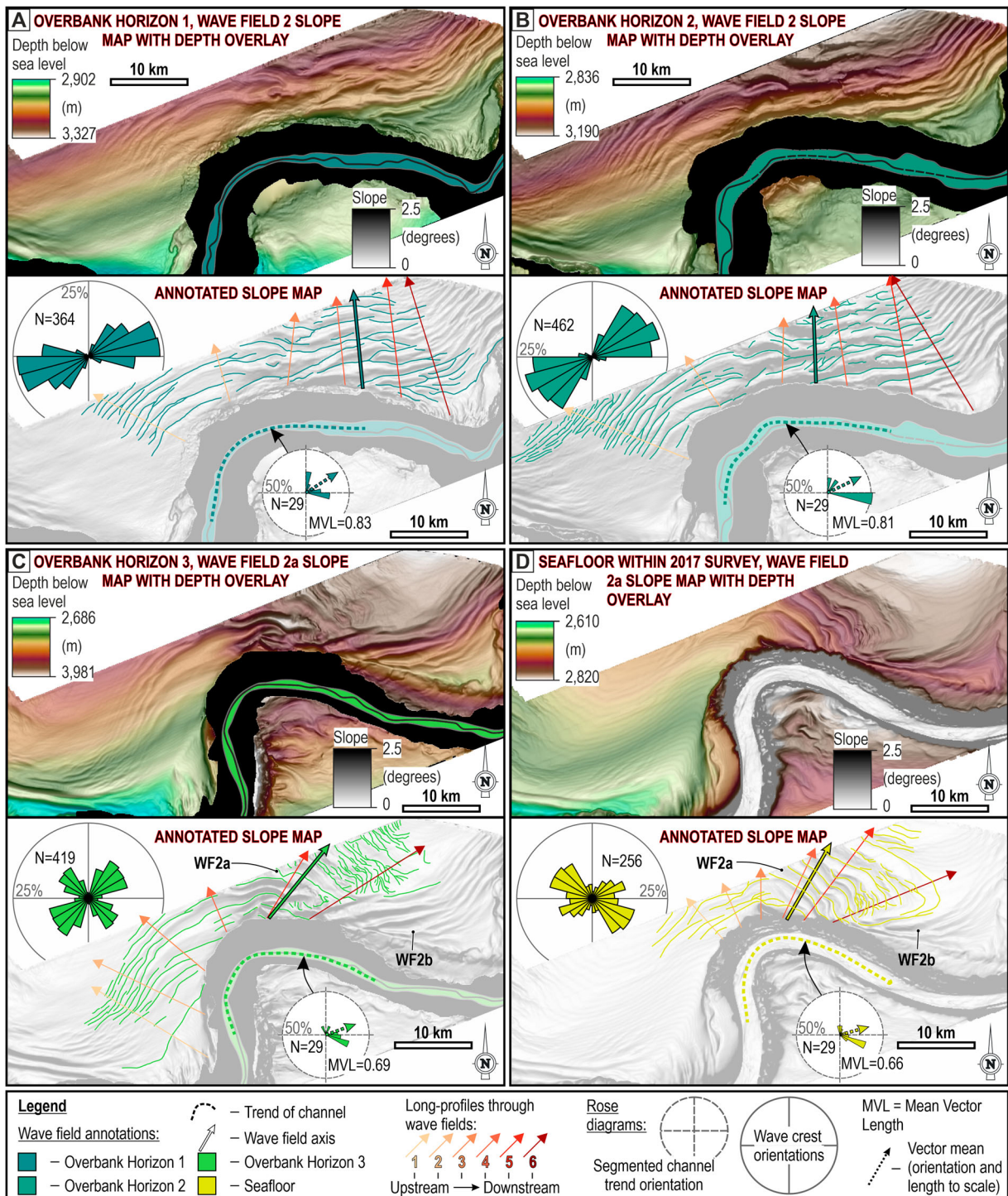


Figure 13. Maps showing the seafloor expression of wave field 2/2a within the extent of the 3D seismic survey on Overbank Horizon 1 (A), Overbank Horizon 2 (B), Overbank Horizon 3 (C), and the seafloor (D). For each horizon, an uninterpreted slope map with depth overlay and an interpreted slope gradient map are displayed. On the interpreted map, the wave crests, the trend of the related channel bend, the locations of the longitudinal profiles shown in Figure 14, including the wave field axis, and two inset rose diagrams showing the (bi-directional) orientations of the wave crest segments and the vector directions of the segmented channel bend trend are highlighted.

In crest-perpendicular cross-section, waves in WF2b exhibit the same sigmoidal reflector geometries with upstream-stacking troughs and crests, similar to outer-bank wave fields (cf. Figures 11C and 16). The crest and trough trajectories of waves in WF2b continue uninterrupted through ~500 m of stratigraphy, and the orientations of their peaks and troughs are concordant through the separation of WF2 into

WF2a and WF2b (Figure 16), suggesting the waves in WF2b have remained relatively static, while waves in WF2a have rotated clockwise. In cross-sections orientated obliquely to wave crests in WF2a and WF2b, the waves from the two fields appear concordant (Figure 16A). However, in sections orientated at higher angles to wave crests in WF2b, there is an abrupt lateral transition between sigmoidal

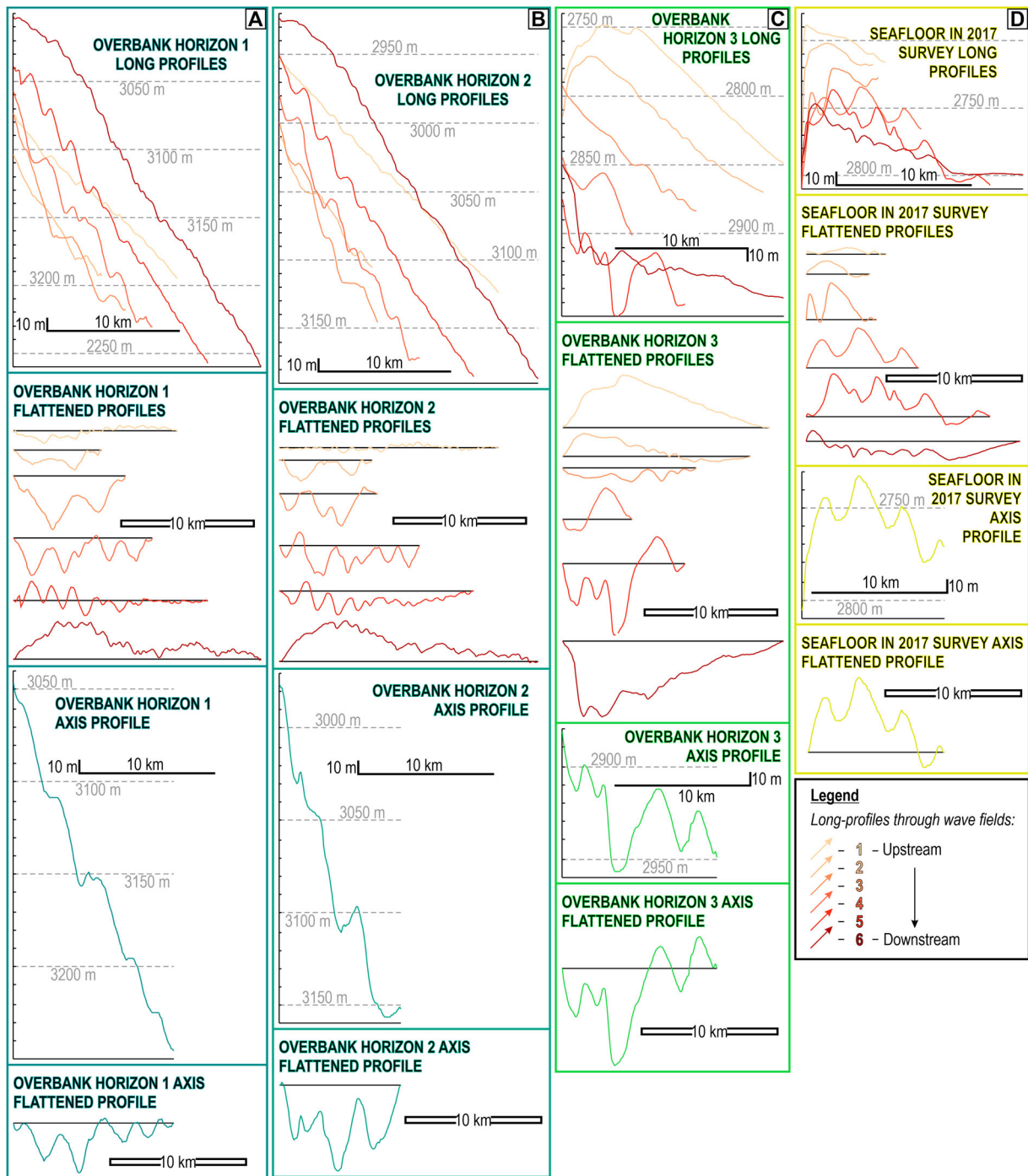


Figure 14. Crest-perpendicular profiles (locations shown in Figure 13) through wave field 2/2a, within the extent of the 3D seismic survey, measured on Overbank Horizon 1 (A), Overbank Horizon 2 (B), Overbank Horizon 3 (C), and the seafloor (D). For each wave field, the six profiles used for the extraction of wave dimensions in Figure 12 are shown in depth and flattened to their upstream and downstream ends, and the wave field axis (profile containing the largest overall wavelength and wave heights), which is also shown in depth and flattened.

wave-bearing reflectors of WF2b that dip away from the channel, to apparently flatter, mounded or tabular reflectors that represent the crest-parallel expression of waves in WF2a (Figure 16B, C). Reflectors (and packages thereof) in WF2a are thicker than contemporaneous reflectors in WF2b, causing the transition between the wave fields to step channelward through progressively shallower stratigraphy, coinciding with the areal growth of WF2a and shrinkage of WF2b (cf. Figure 15C and D). This transition is marked by

a subtle trough (Figure 15D), at which reflectors associated with both wave fields terminate, although the onlap of reflectors in WF2a onto those in WF2b may be mis-interpreted (Figure 15B, C).

Interpretations

Accompanying the expansion of bend 4, WF2 divided into distinct outer-bend (WF2a) and inner-bend (WF2b) fields as overspill on the outer-bank of bend

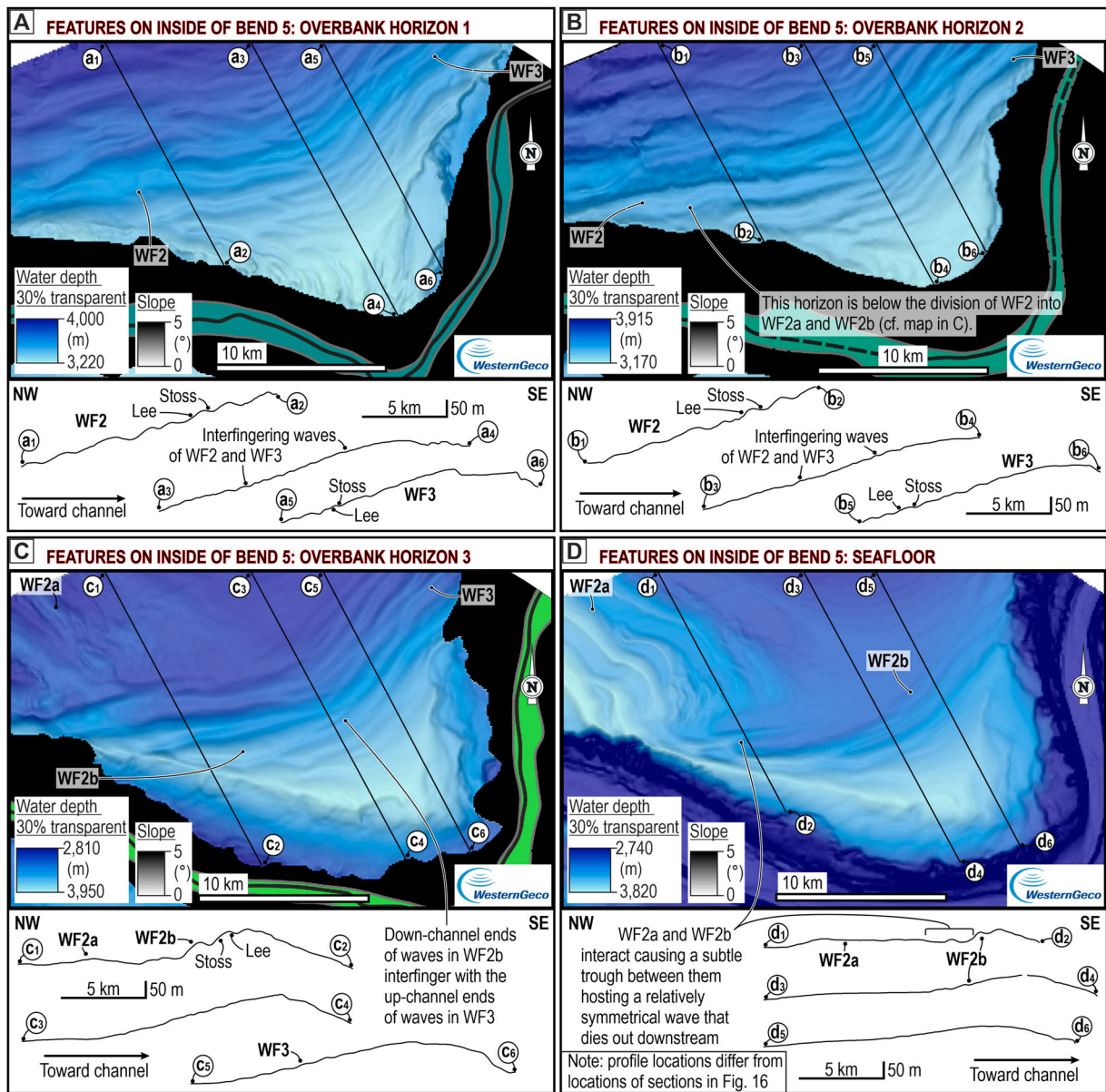


Figure 15. A–D, Slope maps with depth overlays centred on wave field 2/2b showing its relationship with field 2a and field 3, and three ~ crest-perpendicular profiles extracted from: Overbank Horizon 1 (A), Overbank Horizon 2 (B), Overbank Horizon 3 (C), and the seafloor (D).

4 became focused downstream of the bend apex due to an increase in the influence of centrifugal force.

Wave crest-perpendicular overbank flow at the location of WF2b is interpreted to have occurred consistently since sediment wave initiation (deeper than Overbank Horizon 1). The waves in WF2b formed and migrated upstream (SSE) through crest-perpendicular, NNW directed overspill on the inside of bend 5, in a similar manner to the outer-bank sediment waves described above. Overspill on inner-bend overbanks flowing away from the apex of bend 5 can only occur on the landward overbank, due to flow enhancement by the Coriolis force. As WF2a separated from WF2b and rotated, an area of flow interaction was generated between the two fields (Figure 17). Thick overspilling flows that traversed WF2a likely spread out due to flow relaxation (Pohl et al. 2019), generating

an ESE directed component of flow at the down-channel end of the wave field. This ESE-directed flow component interacted with NNW-directed flow traversing WF2b, hindering the development of sediment waves, and forming a trough in which flow originating from both wave fields travelled ~NE (Figure 17A, B, D). Such troughs may represent areas of higher velocity, and potentially contain deposits of coarser grain size.

Based on the thicknesses of contemporaneous reflector packages (Figure 17B), sedimentation rates in WF2a are interpreted to be higher than in WF2b. As WF2a expanded, the outer-levee gradient on the landward channel margin was progressively healed. The disappearance of the up-channel part of WF3 and establishment of a large, waveless area likely occurred as combined overbank flow from WF2a and WF2b became dominant, inhibiting channel-

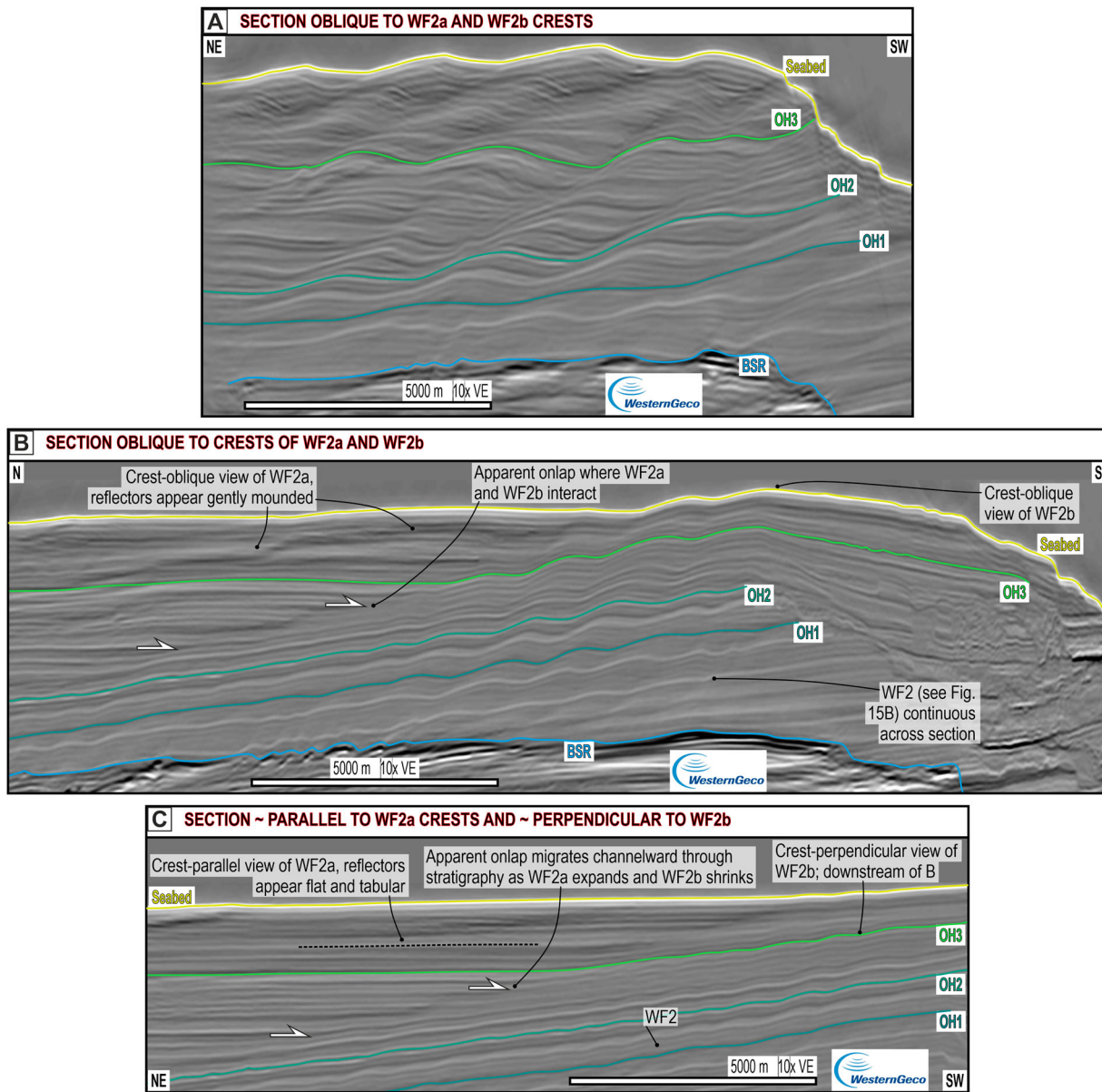


Figure 16. Annotated seismic sections at different angles to the wave crests in wave field 2a and 2b: **A**, is orientated oblique ($\sim 45^\circ$) to crests in both fields, **B**, is orientated oblique to crests in both fields, but at a higher angle ($\sim 70^\circ$) to crests in field 2b, and a lower angle to those in field 2a, **C**, is orientated \sim perpendicular to crests in field 2b and \sim parallel to those in field 2a. Differences in sediment wave height and wavelength are related to the profile locations at different positions along the channel. Note that these sections do not correspond to the profile locations in Figure 15.

perpendicular unidirectional flow on the up-channel outer-overbank of bend 6 (the formative bend of WF3) (Figure 17A, B); down-channel focusing of overspill accompanying the expansion of bend 6 likely augmented this process. Some flow from WF2a and WF2b likely re-enters the channel at the down-channel end of WF2b; much of the sediment is, however, interpreted to be deposited in the flat areas on the up-channel outer-overbank of bend 6 (Figure 17A, B, C).

Inner-bend waves on oceanward channel margin

Observations

Sediment waves are also present on the oceanward margin, on the inner-overbanks of bends 4, 6 and 10

(Figure 18A, B, C). Oceanward inner-bend waves are observed on the seafloor (Figure 18A) and within Overbank Horizon 3 (Figure 18D); they are likely present in deeper stratigraphy (to depths below Overbank Horizon 1) but their 3D geometries are uncertain. The crests of these waves are typically oriented SW-NE to NW-SE at the up-channel end of the field, where they are aligned at orientations sub-perpendicular to oblique to the channel. They curve down-channel and are typically oriented E-W to NW-SE at the down-channel end of the field, where they are aligned subparallel to oblique to the channel (Figure 18). On the inner-overbank of bend 4, at their up-channel end, the troughs of these waves form depressions in the oceanward channel-wall on the straight reach between the apices of bends 3 and 4, reaching over 50 m deep where they intersect the

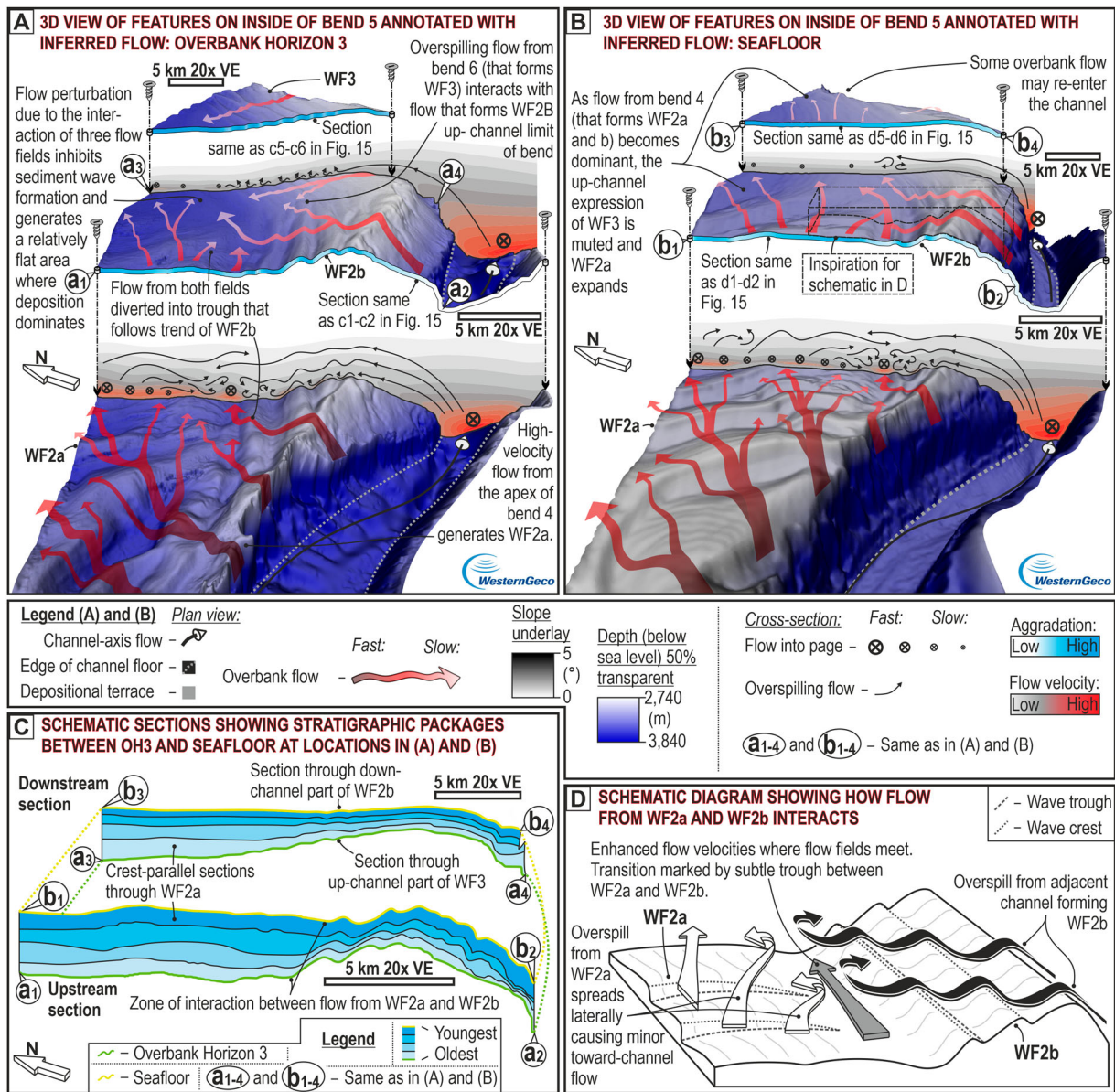


Figure 17. A, Part of Overbank Horizon 3 (same as shown in Figure 15C) displayed in 3D looking down-channel over the inner-overbank of bend 5, annotated with interpreted overbank flow orientations and velocities, and locations of aggradation. **B**, Part of the seafloor (same as shown in Figure 15D) displayed and annotated in the same way as **A**. **C**, Interpreted seismic sections through the locations displayed in A and B, showing the thickness of depositional packages between Overbank Horizon 1 and the seafloor, highlighting an overall down-channel decrease in package thickness and that reflector packages associated with wave field 2a are thicker than those of equivalent age in field 2b. **D**, Schematic section showing the interpreted nature of overbank flow interaction between wave fields 2a and 2b.

channel-wall (Figure 19A, B). The wavelengths and heights of these waves decrease down-channel, and waves branch to form multiple, smaller waves (Figures 18A, B, C, and 19A, B).

In wave crest-perpendicular cross-sections, at their up-channel end, the waves exhibit sigmoidal geometries similar to those observed in waves on the landward margin (cf. Figures 11C and 16 with Figures 18E and 19C). However, on the oceanward margin the wave troughs and crests stack vertically and away from the channel (S to SE), with thicker reflectors on their lee sides, which dip away from the channel (Figure 18E, F).

At the top of packages of terrace deposits, relatively tabular reflectors that form the main body of the terrace transition vertically into lenticular packages of reflectors that are thickest (up to 20 m) immediately channelward of the adjacent terrace-bounding surface (Figure 18E, F). These reflectors thin abruptly (over tens to a couple of hundred metres) away from the channel and terminate against their adjacent terrace-bounding surface, and gradually thin and pinch out (over hundreds of metres to two kilometres) toward the channel. The thickest part of these lens-like reflectors stacks vertically and away from the channel (southward) (Figures 18E, F and 19C). Through

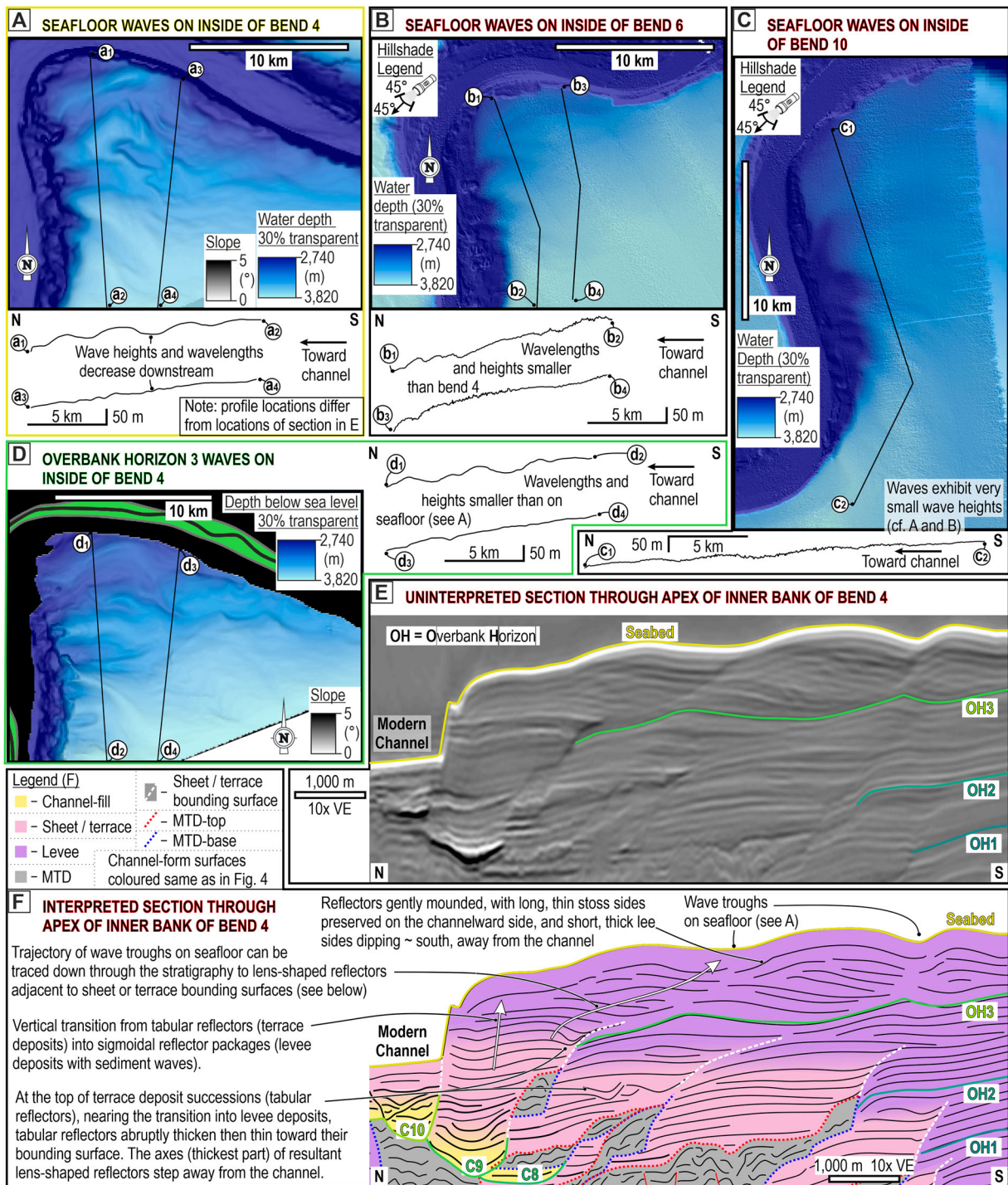


Figure 18. A–C, Seafloor maps displayed as slope (A), or hillshade (B and C) maps with depth overlays, showing inner-bend waves on the oceanward margin, on the insides of bends 4, 6 and 10; crest-perpendicular profiles are also included. D, Slope map with depth overlay showing the waves on the inner-overbank of bend 4 on Overbank Horizon 3; two ~ crest perpendicular profiles included. E, Annotated seismic section and F, interpreted line drawing thereof, showing the seismic expression of the waves on the inner-overbank of bend 4 orientated perpendicular to the wave crests.

progressively shallower stratigraphy, the deepest part of these lens-like reflectors transition into the troughs of the waves observed on the seafloor and Overbank Horizon 3; the reflectors themselves transition into the thick lee sides of the waves near the seafloor (Figure 18E, F). The terrace-bounding surfaces, the deepest parts of lens-like reflectors, and the wave troughs follow a common trajectory that exhibits a

progressively gentler inclination up-stratigraphy and away from the channel (Figure 18E, F). Small waves in the down-channel parts of the field are relatively symmetrical, and do not appear to exhibit distinct differences in reflector geometries on their lee and stoss sides (Figure 19C), although this could be due to geometric variability being below the resolution of the data.

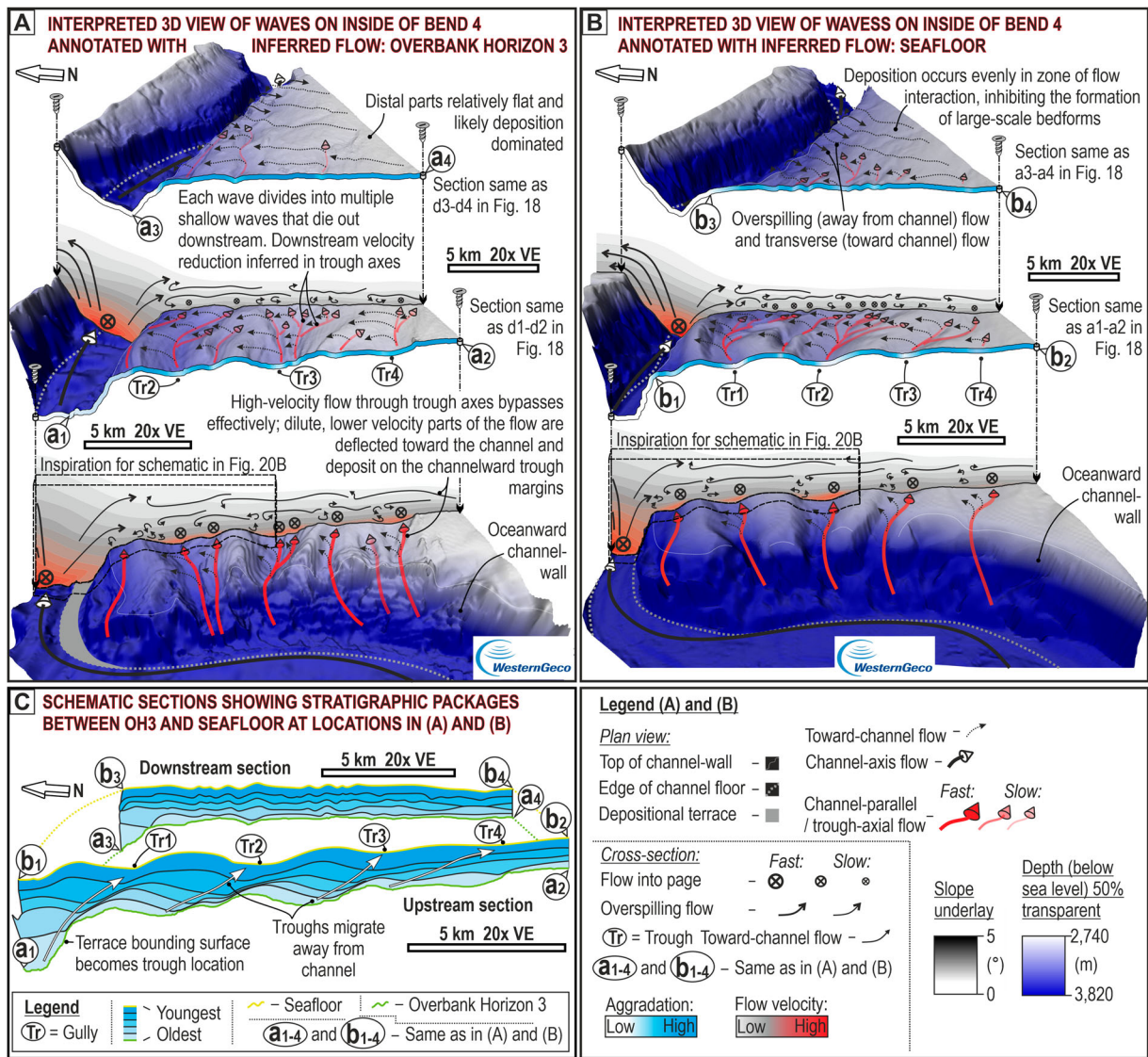


Figure 19. A, Interpreted part of Overbank Horizon 3 (same as shown in Figure 18D) displayed in 3D looking down-channel over the inner-overbank of bend 4, annotated with interpreted overbank flow orientations and velocities, and locations of aggradation. **B**, Interpreted part of the seafloor (same as shown in Figure 18A) displayed and annotated in the same way as **A**. **C**, Interpreted seismic sections through the locations displayed in **A** and **B**, showing the thickness of depositional packages between Overbank Horizon 1 and the seafloor, highlighting an overall down-channel decrease in the sediment wave wavelengths and heights.

Interpretations

Overspill on the oceanward margin is enhanced in the straight channel section between bends 3 and 4 by the influence of centrifugal force downstream of the apex of bend 3. The point of maximum overspill may have also been shifted further down-channel by the influence of the Coriolis force, shifting the point of maximum shear stress on the outside of bend 3 further down-channel. Higher velocity and potentially coarser-grained parts of the overbank flow on the inner-overbank of bend 4 were funnelled through the wave troughs that form depressions in the channel wall (Figures 19A, B and 20A, B). On the channel overbank, higher concentration, higher velocity, dominantly bypassing parts of the overbank flow (McArthur et al. 2020) travel through the axis of the wave troughs. However, a more dilute component of flow, generated dominantly by deflection due to the

Coriolis force and, potentially aided by flow reflected off the Chatham Rise and the subducting plate, and the influence of the DWBC, flows toward the channel (Figure 20A). This transverse component of flow leads to faster deposition on the lee sides of the waves (away from channel), than on the stoss sides; deposition in the axis of troughs is suppressed by the axial flow component (Figures 19A, B and 20B). Through time, these processes build the sigmoidal reflector geometries and troughs that stack away from the channel that are observed in the subsurface (Figure 19C); this migration pattern differs from the interpreted toward-channel migration of waves on the oceanward overbank (Figure 16).

The aforementioned waves evolve from terraces. Terraces aggrade faster than levees in the Hikurangi Channel, as evidenced by observed vertical transitions from terrace to overbank deposits (Figure 18E, F; Tek

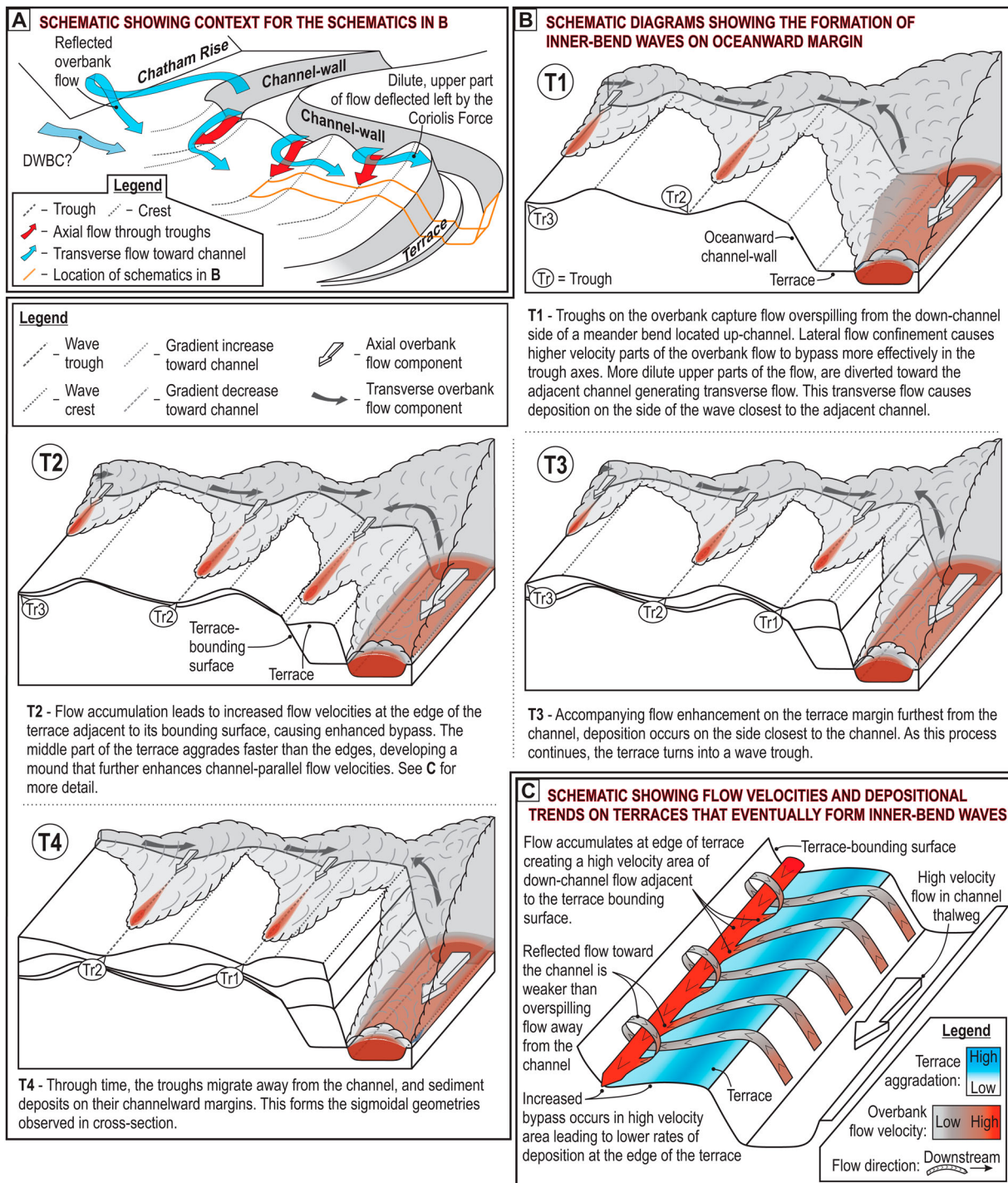


Figure 20. Diagrams showing the formation and evolution of inner-bend waves on the oceanward overbank, specifically on the inside of bend 4. **A**, Three-dimensional schematic showing the context of the inner-bend waves detailed in B, and the cause of transverse flow toward the channel and its relationship with trough-axial flow. **B**, Detailed schematic diagrams (location on Figure 19A and B; stratigraphic evolution based on upstream section in Figure 19C; note perspective change from Figure 19 to looking up-channel) demonstrating how the sediment waves evolve from terraces, and how the interaction between axial flow through the wave troughs and transverse flow toward the channel causes sediment wave migration away from the channel. **C**, Schematic showing how flow accumulation against the terrace-bounding surface generates a high-velocity component of down-channel flow leading to bypass at the terrace edge and mounding in the centre.

et al. 2021). Flow on terraces is complex, commonly comprising a primary component that flows down-channel and away from the channel, and a secondary component that flows down-channel and toward the channel after being reflected off the terrace-bounding surface (Figure 20C; Hansen et al. 2015). When a terrace has aggraded to near the height of its adjacent

levee, the primary flow component dominates the reflected flow component, causing flow convergence (*sensu* Kneller 1995) adjacent to the terrace-bounding surface. Accumulative flow leads to a high-velocity component of flow that travels down-channel, parallel to the confining terrace-bounding surface (Kneller and McCaffrey 1999), where erosion and/or bypass is

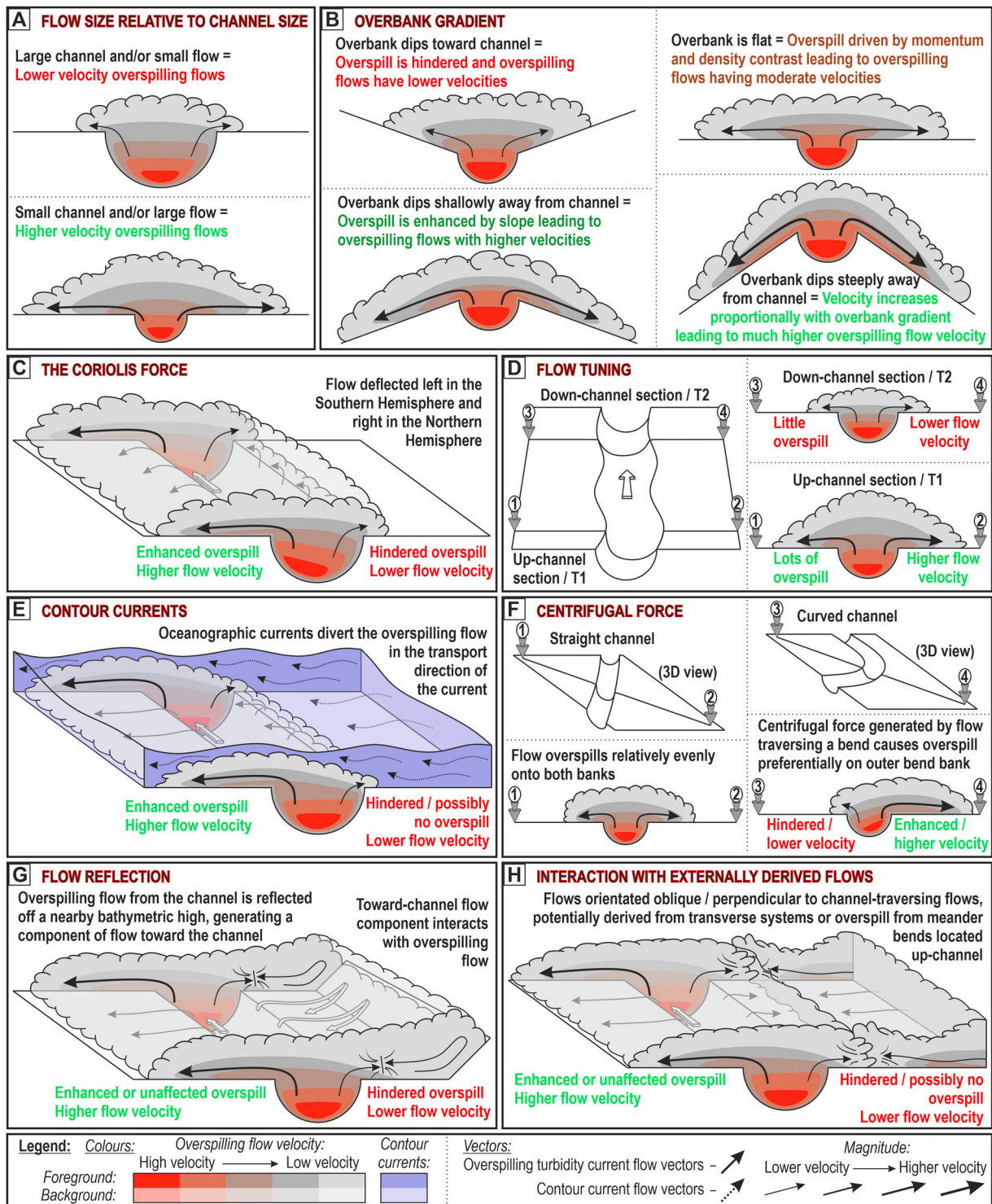


Figure 21. Schematic diagrams showing eight of the nine processes interpreted to control overspill from the Hikurangi Channel: **A**, flow size relative to conduit size, **B**, overbank gradient, **C**, flow tuning, **D**, the Coriolis force, **E**, contour current, **F**, centrifugal force, **G**, flow reflection, **H**, interaction with externally derived flows. The interaction of flows originating from different parts of the channel is demonstrated in [Figure 23](#).

enhanced, and deposition is hindered ([Figure 20C](#)). This process generates mounded reflectors on the terraces and concave-up surfaces adjacent to terrace-bounding surfaces, which are filled with lens-like reflectors (T2 in [Figure 20B](#)). High-velocity down-channel flow is also sheltered from a Coriolis-induced transverse component of overbank flow (potentially influenced by other processes) that travels toward the

channel (responsible for deposition on the lee sides of the waves; see above) by the terrace-bounding surface. As the terrace aggrades further, the influence of this transverse flow component becomes greater. As such, the mounded, middle part of the terrace becomes an inner-overbank wave crest, and the area of enhanced bypass adjacent to the terrace-bounding surface becomes a trough (T3 and T4 in [Figure 20B](#)).

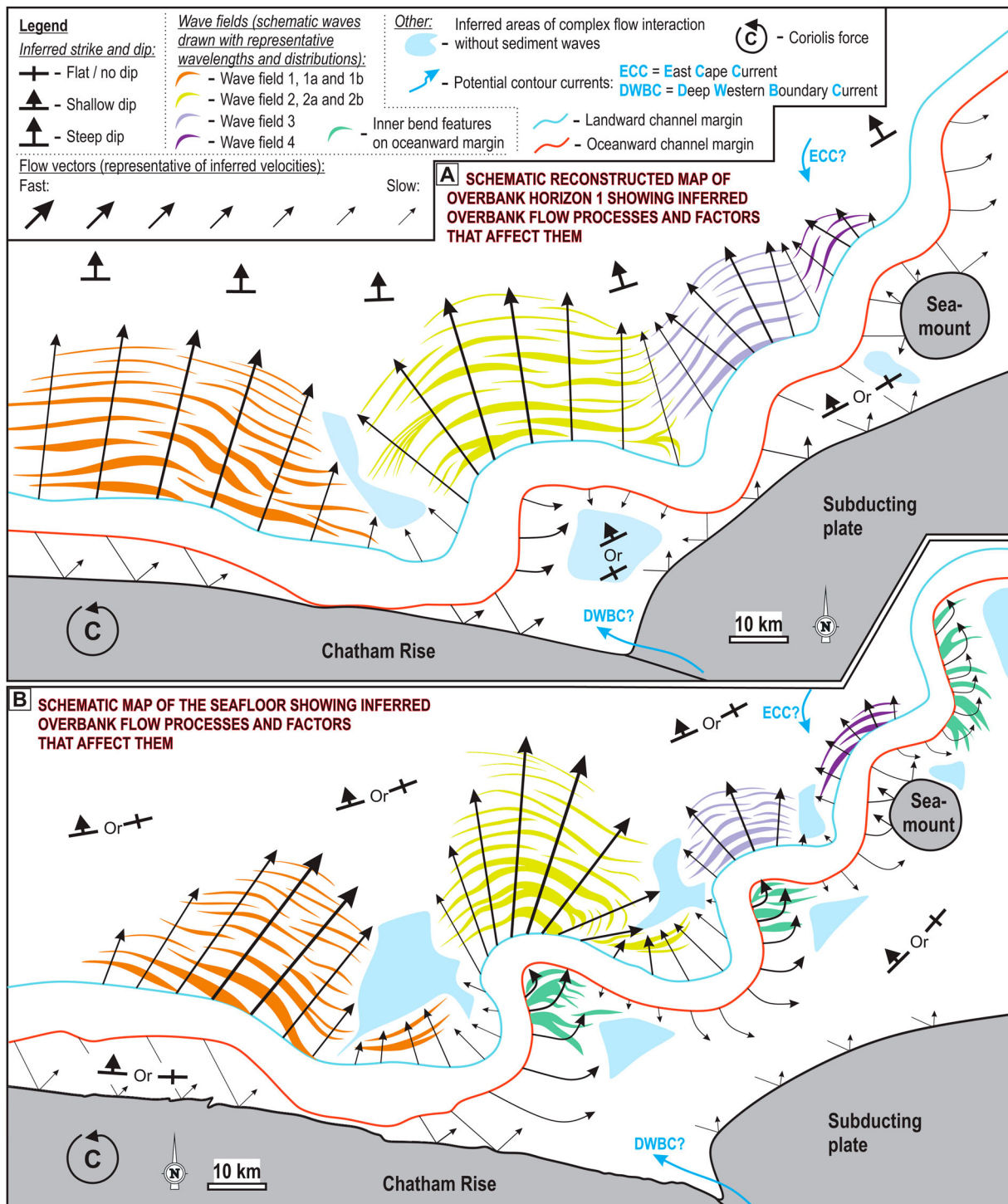


Figure 22. Schematic diagrams showing the distribution of sediment waves and interpreted overbank flow in the deep stratigraphy, on Overbank Horizon 1 (A), and on the seafloor (B).

Further down-channel, the influence of flow through the axis of the troughs is interpreted to diminish progressively, causing fanning of the waves and rotation of the wave crests to be oriented subparallel to the reach of channel downstream of the bend apex. The less well-pronounced waves in down-channel parts of the field are interpreted to have formed dominantly by the transverse, toward-channel component of flow (Figure 19). The more symmetrical shape of these waves suggests that overbank flow away from the channel on the up-channel outer-

overbank of bend 5 may have generated a competing component of flow, impeding strong unidirectional flow and leading to more even deposition (Figure 19).

Discussion

Controls on overspill processes on the overbanks of the Hikurangi Channel

Nine factors that control the nature of overbank flow and the resultant overbank depositional architecture

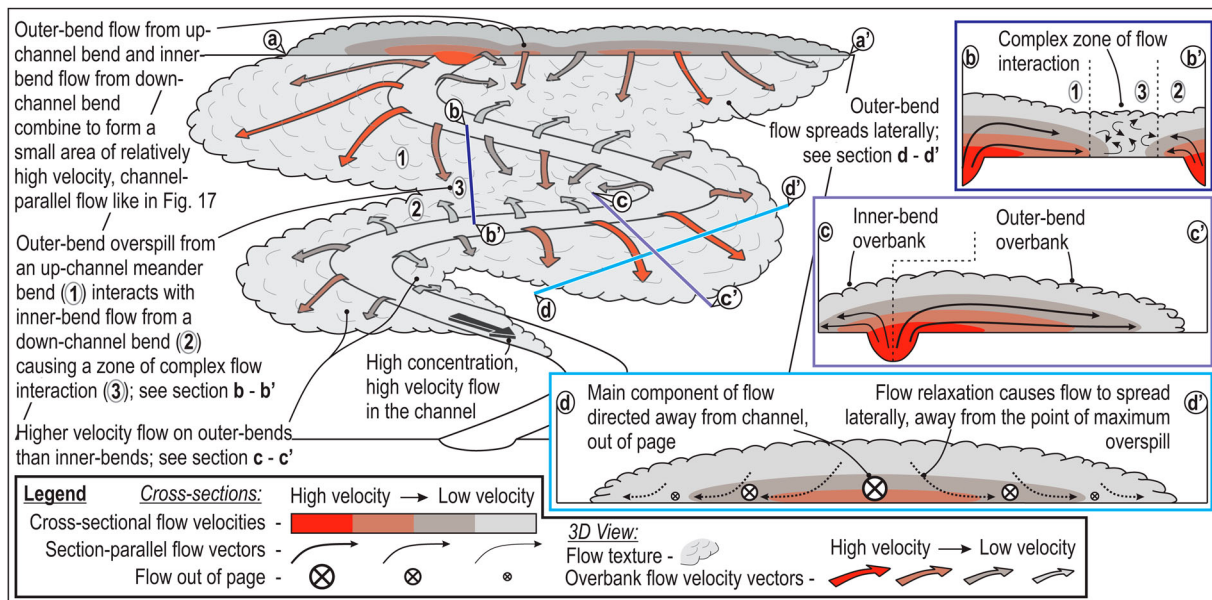


Figure 23. Schematic diagram showing how overbank flow originating from different parts of a channel interacts on the overbanks.

of the Hikurangi Channel have been identified (Figure 21).

Flow size versus conduit size

The thickness of a turbidity current relative to the depth of its host conduit is a fundamental control on the magnitude and velocity of overbank flow. Larger flows generate thicker and likely higher velocity overbank flow, meaning coarser parts of stratified flows can escape the conduit (Figure 21A; Dennielou et al. 2006).

Overbank gradient

Flow velocity may be enhanced on channel overbanks with steep outer-levee gradients that slope away from their conduit and hindered on overbanks that slope toward the channel (Figure 21B; Kane et al. 2010; Nakajima and Kneller 2013). In the studied reach of the Hikurangi Channel, the oceanward overbank is horizontal, or slopes toward the channel throughout the studied stratigraphy. This appears to have hindered overbank flow and inhibited the formation of sediment waves on the oceanward overbank (Figure 22). On the landward margin, the outer-levee gradient is interpreted to have shallowed progressively as slope-traversing drainage networks were established, and overbank flow downstream of the apex of expanding bends acted to redistribute sediment in the trench, leading to a largely flat trench-floor and gently-sloping to flat outer-levees (Table 2, Figures 3B and 22).

Flow 'tuning'

A systematic down-channel decrease in the magnitude and velocity of overspill from the Hikurangi Channel is attributed to the process of flow 'tuning'. This arises from the loss of material from the dilute, upper parts

of flows in up-channel locations, causing the range of flow heights to decrease down-channel as flows progressively lose material, with thicker flows losing more than thinner-ones (Figure 21C; Mohrig and Buttles 2007; Kelly et al. 2019). Flow tuning has generated a down-channel decrease in the size of the outer-bend wave fields (Figure 22).

The Coriolis force

The leftward deflection of overbank (and potentially in-channel) flow characteristic of the Coriolis force in the southern hemisphere (Figure 21D; Klauke et al. 1998; Cossu et al. 2015) has exerted a significant control on overbank architecture throughout the depositional period along the studied channel reach (Figure 22); this control was also recognised by Lewis and Pantin (2002). This flow deflection contributed to the generation of large, outer-bend wave fields solely on the landward overbank. It was also instrumental in the generation of transverse flow toward the channel that forms inner-bend waves on the oceanward channel margin (Figures 19 and 22), and in maintaining continual flow away from the channel on inner-bend overbanks on the landward margin (Figures 17 and 22).

Contour currents

Contour currents may locally hinder overspill that flows counter to them and augment overspill in the same direction (Figure 21E; Miramontes et al. 2020). While the locations and orientations of contour currents in the studied part of the Hikurangi Trench are poorly constrained, two currents have potentially affected the study area at different times. Lewis and Pantin (2002) inferred that a shallow branch of the

DWBC flowed W along the northern edge of the Chatham Rise, which controlled the formation of inner-bend sediment waves on the oceanward margin (Figures 2 and 22). The detailed observations made herein allow for the interpretation that the DWBC helped generate a toward-channel component of overbank flow that contributes to the formation of inner-overbank waves (Figure 20). However, the presence of similar waves on the inside of bends 6 and 10, where the DWBC would be unlikely to act, suggests that its effect may have been relatively minor. Furthermore, the DWBC is not observed to be presently active in the study area (Fernandez et al. 2018), meaning its potential effect would vary temporally. The ECC, in contrast, is currently active and likely flows SE across the channel in the study area, but the location of the crossing is unclear (Figure 2). If the ECC crosses the down-channel parts of the studied channel reach, it may be partially responsible for the down-channel decrease in wave field size on the landward overbank (Figure 22). If the ECC crosses the channel in a location further up-channel, its effects are likely negligible and are not recorded by the sediment wave distributions. Bailey et al. (2020) tentatively interpreted that a bottom current crossed the Hikurangi Channel at bend 4, which they inferred locally modified the channel and overbank wave field. However, analysis of the morphology and distribution of these sediment waves herein suggests they are more likely related to overbank flow, meaning that if the ECC crosses the channel at bend 4 it is unlikely to significantly affect overbank sediment wave development. Definitively determining the influence of contour currents on overbank sedimentation in the Hikurangi Trench requires additional oceanographic data.

Centrifugal force

Accompanying a channel bend's expansion, centrifugal force causes a focusing of overspill downstream of bend apices (Figure 21F; Timbrell 1993; Kane et al. 2008). Through time, as the channel became more sinuous, the wave fields on the landward channel overbank became spatially separated from one another, and some divided into distinct outer-bend and inner-bend fields (Figure 22). The plan-view morphologies and distributions of wavelengths and wave heights in each field also changed concomitantly with increased channel sinuosity (Figure 22). The effect of centrifugal force on sediment wave geometries on the seafloor in the study area was originally noted by Lewis and Pantin (2002).

Flow reflection

The Chatham Rise and the less prominent subducting Pacific plate generate seafloor topography that runs along the oceanward margin of the channel. Overbank flow reflects off this topography, generating

(potentially in conjunction with other factors) a component of flow toward the channel (Figures 21G and 22). This toward-channel component of flow may inhibit the formation of outer-bend sediment waves on the oceanward overbank, and contribute to the formation of inner-bend waves on the oceanward overbank (Figure 20). The thickness of contemporaneously formed reflector packages (Table 2 and Figure 3) suggest deposition rates are generally higher on the flat trench floor than on the steep Chatham Rise and subducting plate. Therefore, largely tabular reflectors were generated, allowing the classification of the oceanward overbank deposits as 'confined external levees' (Table 2; Clark and Cartwright 2011).

Interaction with externally derived flows

The interaction with turbidity currents of different origins (Figure 21H; Okon et al. 2021) may exert a control on overbank flow in the Hikurangi Channel. The dilute, distal parts of SE flowing, slope-traversing turbidity currents may interact with distal, NW flowing overbank flow near the subduction front (Figure 2). Interaction of these turbidity currents may reduce the velocity of unidirectional overbank flow and restrict the size of outer-bend wave fields (Figure 22). Alternatively, flow of these different origins may not interact, but their deposits may stack compensationally; more data are needed to determine which process is dominant in the Hikurangi Trench. Regardless of whether the individual flows interact, combined deposition from slope-traversing and overbank flows may occur over the entire trench floor (outside of the channel), suppressing the development of steep outer-levee gradients and leading to a relatively flat trench floor (Table 2, Figures 3 and 6). In systems where two contemporaneously active channels run parallel to one another, overspill derived from the two channels may also interact on their mutual overbank, causing flow complexity.

Interaction of overspill from different locations

Overbank flows originating from different locations along the channel may generate areas of complex flow interaction, inhibiting the development of sediment waves. In the Hikurangi Channel, overspill down-channel of a landward facing bend may interact with lower velocity up-channel overspill from the next down-channel (landward facing) bend (Figures 22 and 23). This interaction could initially occur due to bend expansion causing a separation of the wave fields and focusing flow on the downstream sides of bends, generating a complex zone of flow interaction (Figure 23). Consistent unidirectional flow does not occur in these zones and consequently they are devoid of sediment waves (Figure 22). Interaction of flow from different bends is likely to be more common in channel systems with relatively flat, laterally-confined overbanks like

the Hikurangi Channel, where the gradient of the outer-levee does not cause overspill to flow consistently away from the channel.

Spatio-temporal variability and interaction of controls

The subsurface architecture and seafloor expression of the studied overbank deposits are a product of the complex interaction between the controls listed above. The effect of most controls will also differ between individual flows as the flow height fundamentally dictates the volume of overspill (Figure 21A); tuning effects may eventually suppress such differences. The influence of some controls, such as the Coriolis force, is also partially dependent on the nature of channel-traversing flows (Cossu et al. 2015; Davarpanah Jazi et al. 2020). Variations in flow thickness and nature can also occur cyclically, in response to sea-level fluctuations and climatic changes (Romans et al. 2016). The effect of some controls, such as contour currents, may also vary over a range of distinct timescales. For example, the ECC is highly variable on interannual and decadal timescales (Fernandez et al. 2018), and the shallow branch of the DWBC invoked by Lewis and Pantin (2002) may only be active during glacial periods. However, the analysis of sediment waves and seismic-scale architecture herein has allowed the spatio-temporal variability of the influence of different controls on net overbank flow and sedimentation over longer timescales to be determined. This helps to mitigate uncertainty related to variability at timescales between individual flows.

Spatial variability in the magnitude at which controls operate is inferred on the seafloor and in the subsurface. Coriolis forcing (Figure 21D) is the only control that is not spatially restricted at the scale of observation, and consistently affects overbank flow across the entire area. The effect of some controls changes up- or down-channel. For example, by definition, flow tuning (Figure 21C) generates a down-channel decrease in the magnitude of overspill. However, some controls, such as centrifugal force (Figure 21F), overbank gradient (Figure 21B) and interaction of overspill from different locations (Figure 23), are inherently linked to the morphology of the channel and its overbanks. As such, they can produce more localised effects and are subject to feedback effects. For example, the influence of centrifugal force is dependent on bend curvature, meaning its effect will vary between adjacent bends (tens of km) (Figure 22). Other controls that present localised effects but are not directly related to channel morphology include contour currents (Figure 21E) and flow reflection (Figure 21A). For example, in this setting flow reflection is likely to influence flow dominantly on the oceanward overbank (Figure 22).

Additionally, as topography generated by the Chatham Rise is steeper, taller, and closer to the channel than the Pacific plate, the strength of reflected flow likely also decreases downstream.

Changes in sediment wave morphology are observed through the studied stratigraphy. These changes are caused by long-term temporal variations in the relative influence of some controls; other controls have affected overbank flow and sedimentation consistently throughout the depositional period. For example, the Coriolis force (Figure 21D) has consistently affected overbank flow and sedimentation throughout deposition (Figure 22). However, the influence of centrifugal force has increased with increasing channel sinuosity. The effect of other controls may have been constant throughout deposition in some areas, but variable in other areas. For example, the effect of toward-channel overbank gradients on the oceanward margin has been constant, whereas the away-from-channel gradient on the landward overbank is interpreted to have progressively shallowed through time, changing its influence on overbank flow (Figure 22).

Multiple controls that influence overbank flow in a given location can either augment or act against one another. For example, on the oceanward overbank the effects of the Coriolis force (Figure 21D), an overbank gradient that sloped toward the channel (Figure 21B), and flow reflecting off the Chatham Rise and the Pacific plate (Figure 21G), combine to generate a component of flow that travels toward the channel (Figures 20 and 22). These three factors counteract the effect of centrifugal force on the oceanward margin, inhibiting the formation of outer-bend sediment waves on the oceanward margin (Figure 22). In addition to separate controls competing for dominance in a given area, the effect of some controls is directly dependent on the presence of others. For example, the interaction of overspill originating from different bends (Figure 23) is effectively dependent on channel sinuosity and the effect of centrifugal force; an increase in sinuosity, and therefore centrifugal force, will consequently increase the interaction of down-channel overbank flow from up-channel bends, and up-channel flow from down-channel bends, leading to a progressive loss of sediment waves in the location of interaction.

Overall, the complex interaction between controls that have affected overspill on different parts of the overbank area consistently through time, vs. those that are temporally variable has led to the complex sediment wave distributions and depositional architectures described herein. It is therefore difficult to rank the importance of all controls. However, granted that overspill is occurring, evidence for leftward flow deflection is observed across the entire overbank area meaning that, while the effects of other controls locally augmented its effects, the Coriolis force is

dominantly responsible for enhanced landward overbank flow and hindered oceanward overbank flow. Through progressively shallower stratigraphy, accompanying an increase in channel sinuosity, the morphologies of the waves on the landward margin have changed accordingly. Therefore, the interaction between Coriolis and centrifugal forcing are interpreted to have produced the most significant effect on overbank sediment wave distribution and overbank architecture, particularly on the landward overbank. These interpretations are generally in accordance with those of Lewis and Pantin (2002).

Inner-bend sediment wave fields

Identification of inner-bend wave fields on both sides of the channel was permitted by using high-resolution bathymetry and 3D seismic data. Inner-bend wave fields on each side of the channel are interpreted to have different mechanisms of formation, but both form as a result of multiple components of overbank flow originating in different locations and travelling in various orientations (Figures 17, 19 and 20). As such, they record more complex patterns of overbank flow and sedimentation than outer-bend waves and the morphologies of their constituent waves do not show simple relationships with the orientations of their formative flows.

Lewis and Pantin (2002) interpreted that waves that migrate away from the channel on the oceanward margin on the inside of bend 4 (this study), were produced solely by westward flowing contour currents (a shallow branch of the DWBC). However, in-depth analysis of these waves and their 3D subsurface architecture suggests that these waves are the product of the complex interaction between two different overbank flow components: some overspilling flow generates an axial flow component that is funnelled through the wave troughs; some is deflected by the Coriolis force, reflected off the Chatham Rise or subducting plate, and possibly influenced by the DWBC, generating a transverse flow component toward the channel (Figures 19 and 20).

On the landward margin, inner-bend sediment wave fields have formed and become separated from wave fields on the outer-overbanks as the shape and distributions of outer-bend wave fields have progressively rotated and migrated down-channel (Figures 7, 9, 13, and 22). The inner-bend waves are formed and maintained by overspill on the inner-overbank of bends, the velocity of which in the study area is augmented by the Coriolis force. However, a subtle trough marks the contact between the outer- and inner-bend wave fields, which is interpreted to funnel relatively high-velocity parts of the flow (Figures 17 and 23); the crests of waves in the outer-bend fields are oriented normal to those in the inner-bend fields.

The separation of outer bend fields and the complexity of inferred flow within them and at their boundary is due to the interaction of flow components originating from different parts of the channel (Figure 23).

Sedimentological implications

The many controls listed above act to control flow processes and the development of sediment waves on the overbank areas of the Hikurangi Channel. The effect each control exerted on the overbank deposit architecture varied along the channel and through time, generating overbank deposits with a complex three-dimensional architecture. These deposits, their trends, and their sedimentary structures, may differ from those portrayed in conventional models derived from studies using outcrop, seafloor, or 2D seismic data.

On the seafloor, the Hikurangi Channel apparently lacks well-defined levees along much of its length. However, this bears no reflection on how effectively channel-traversing flows overspill, nor the nature of the channel and overbank deposits in the subsurface. It is merely a result of deposition by slope-traversing flows derived from the subduction margin and overspilling from the Hikurangi Channel occurring across the floor of a laterally-confined trench, and effectively filling the lateral accommodation space therein (Figure 3); the Hikurangi Channel is highly aggradational (cf. Casciano et al. 2019). The fact that highly aggradational channels such as the Hikurangi Channel can be bordered by effectively flat overbank areas on the seafloor means the seafloor profile of submarine channel overbanks can be an unreliable predictor of subsurface channel and overbank architecture.

The orientation of overbank flow from the Hikurangi Channel is interpreted to vary substantially. On the oceanward and landward overbanks, the interaction of flows from different bends, flow reflection, and the Coriolis force generate areas with complex multidirectional flow. Deposits in these areas may exhibit highly variable palaeocurrents and may contain 'combined flow' bedforms such as hummocky cross-stratification (Muzzi Magalhaes and Tinterri 2010). In outcrop, palaeocurrent variability has been used to distinguish 'internal levees' or 'terraces', which typically exhibit highly variable palaeocurrents, from 'external levees', which exhibit less variability (Kane and Hodgson 2011). However, in outcropping confined channel systems with low overbank gradients, that are analogous to the Hikurangi Channel, this criterion may not be reliable.

In high latitude systems, the dominance of Coriolis forcing upon cross channel flow results in preferential deposition along one channel overbank (Cossu et al. 2015) and hinders sinuosity development (Peakall et al. 2012). In low latitude settings, Coriolis forces

are negligible, and flow dynamics are dominated by centrifugal forces, leading to preferential overspill at bend apices on opposing sides of the channel, in successive bends (Keevil et al. 2006; Cossu and Wells 2010). The overbank architecture of the mid-latitude (*sensu* Menard 1955; Savoye et al. 1993) Hikurangi Channel displays evidence of the effect of both Coriolis and centrifugal forces on overbank architecture. The relative influence of these competing controls varied through time as a result of changing channel morphology, generating a more complex architecture than can be predicted by either of the aforementioned end member controls.

On the seafloor and in the subsurface of the Hikurangi Channel, evidence for the interaction of overbank flow and deposition from different locations along the channel are observed (Figure 23). Interacting packages of overbank deposits can thin toward, and interfinger with, each other (Table 2 and Figure 16). In 2D seismic sections or in outcropping sections, these depositional architectures may be interpreted to be derived from an extra-channel source. Evidence for the interaction of contemporaneous overspill from different parts of the channel (Figure 23) is also observed. In outcrop or core, these areas of interaction may exhibit complex paleocurrent variability and contain complex combinations of sedimentary structures and architectures that appear uncharacteristic of classic levee deposits.

Therefore, in the Hikurangi Channel, and probably in channels in other confined basins in mid-latitudes, simple models explaining bed thicknesses and sandstone distribution, palaeocurrent orientations, and sedimentary structures cannot be applied universally. This has implications for the interpretation of overbank deposits and therefore palaeogeographic reconstructions in outcropping ancient channel systems, but also for categorising channel types and inferring flow processes in channels and on their overbanks from bathymetric data alone.

Conclusions

Integration of high-resolution bathymetry, 2D, and 3D seismic data is used to investigate the controls on overbank flow processes and depositional architecture on the overbank areas of the Hikurangi Channel. Novel techniques for the quantitative analysis of sediment wave orientations and morphologies are conducted on the seafloor and on three, regionally-traceable subsurface horizons, and are used to interpret the three-dimensional subsurface architecture, and infer overbank flow processes.

Nine factors are interpreted to have controlled overbank flow processes on the overbanks of the Hikurangi Channel: flow size versus conduit size, overbank gradient (magnitude and orientation), flow tuning, the Coriolis force, contour currents, flow reflection,

centrifugal force, interaction with externally derived flows, and interaction of overspill from different locations along the channel. These controls mutually interact, and their relative importance has varied significantly throughout the depositional period, and in different parts of the studied overbanks, generating complex patterns of overbank flow and sedimentation.

In deeper stratigraphy the Hikurangi Channel was straighter and was bordered on the landward margin by four sediment wave fields, with no wave fields preserved on the oceanward margin. Overspill that formed sediment waves on the landward margin occurred along the whole studied channel reach, and flowed away from the channel over relatively steep external levees; overbank flow velocities decreased down-channel and increased toward the apices of the then poorly-developed bends. Sediment wave formation was inhibited on the oceanward and enhanced on the landward margin by the combined effects of the oceanward channel overbank sloping toward the channel, flow reflection off the Chatham Rise and the subducting plate, and leftward flow deflection by the Coriolis force.

Through progressively shallower stratigraphy, focusing of overbank flow downstream of bend apices led to the spatial separation of the four wave fields on the landward margin, the division of the most up-channel two wave fields into distinct inner-and outer-bend fields, and the development of inner-bend waves on the oceanward margin. These morphological trends chiefly arose due to an increase in channel sinuosity, augmented by a reduction in gradient on the landward margin as the trench-floor became flat; other controls such as the interaction of overbanks flow with slope-traversing turbidity currents near the subduction margin, and two contour currents (the East Cape Current and the Deep Western Boundary Current) may also have exerted some control.

This study builds on work by Lewis and Pantin (2002). However, detailed observations from high-resolution data have permitted new quantitative analysis of wave morphologies and distributions, and interpretation of how the influence of each control has varied through time. It has also allowed the novel identification of distinct inner-bend wave fields. The nature of inner-bend fields on the landward margin is controlled by the interaction of Coriolis-enhanced overspill on wave-hosting inner-bends, and flow from the down-channel outer-bend overbank of the adjacent, up-channel bend. Inner-bend wave fields on the oceanward margin originate as terraces then evolve and migrate through the combined effects of axial flow funnelled through the wave troughs, and transverse flow toward the channel created by dilute overspill reflected off the Chatham Rise or subducting slab, and deflected by the Coriolis force.

Some or all of the controls on overbank flow and overbank deposit architectures identified in the Hikurangi Channel are common to most modern and ancient channel systems, and particularly those in mid-latitude and/or confined basins. This work has implications for the interpretation of overbank flow processes from seafloor data, and palaeoenvironmental reconstructions from ancient, outcropping overbank deposits.

Acknowledgements

This work was funded by Turbidites Research Group; we thank sponsors AkerBP, CNOOC, ConocoPhillips, Murphy, OMV, and OXY. Schlumberger WesternGeco are thanked for access to the seismic data used in this study. Multibeam bathymetry and backscatter data displayed are made available for download by NIWA, and can be obtained from NZPM. Marta Ribó is thanked for insightful discussions that helped improve the methodologies used herein. We thank Emma Morris and an anonymous reviewer for their thorough reviews that have improved the quality of the manuscript, and Editor Lorna Strachan for handling the manuscript.

Disclosure statement

No potential conflict of interest was reported by the author(s).

Funding

This work was supported by China National Offshore Oil Corporation; ConocoPhillips; Murphy; Oxy; Aker BP; OMV.

Data availability statement

The data that support the findings of this study are available upon application to Schlumberger WesternGeco (<https://www.slb.com/companies/westerngeco>). Restrictions apply to the availability of these data, which were used under license for this study. Bathymetry data available from New Zealand Petroleum and Minerals as part of their 2016 datapack (<https://www.nzpam.govt.nz/maps-geoscience/petroleum-datapack/>).

References

- Babonneau N, Savoye B, Cremer M, Bez M. 2004. Multiple terraces within the deep incised Zaire Valley (ZaiAngo Project): are they confined levees? In: Lomas SA, Joseph P, editor. Confined turbidite systems. Geological Society of London Special Publication, Vol. 222. London: The Geological Society of London; p. 91–114.
- Bailey WS, McArthur AD, McCaffrey WD. 2020. Distribution of contourite drifts on convergent margins: examples from the Hikurangi subduction margin of New Zealand. *Sedimentology*. 68(1):296–323.
- Ballance PF. 1975. Evolution of the India-Pacific plate boundary in North Island, New Zealand. *Bulletin of the Australian Society of Exploration Geophysicists*. 6:58–59.
- Barnes PM, Lamarche G, Bialas J, Henrys S, Pecher I, Netzeband GL, Greinert J, Mountjoy JJ, Pedley K, Crutchley G. 2010. Tectonic and geological framework for gas hydrates and cold seeps on the Hikurangi subduction margin, New Zealand. *Marine Geology*. 272:26–48.
- Barnes PM, Wallace LM, Saffer DM, Bell RE, Underwood MB, Fagereng A, Meneghini F, Savage HM, Rabinowitz HS, Morgan JK, et al. 2020. Slow slip source characterized by lithological and geometric heterogeneity. *Science Advances*. 6(13):eaay3314:1–10.
- Bell D, Stevenson CJ, Kane IA, Hodgson DM, Poyatos-Moré M. 2018. Topographic controls on the development of contemporaneous but contrasting basin-floor depositional architectures. *Journal of Sedimentary Research*. 88(10):1166–1189.
- Bland KJ, Lamarche G, Anderson O, Barnes PM, Black J, Bowden D, Chiswell S, Crutchley G, Gorman R, Mountjoy J, et al. 2014. Pegasus basin petroleum prospectivity screening report. GNS Science Consultancy Report 2014/103, NZP&M, Ministry of Business, Innovation & Employment (MBIE), New Zealand Unpublished Report PR(CR2014-103). p. 1–139.
- Cardozo N, Allmendinger RW. 2013. Spherical projections with OSXStereonet. *Computers and Geosciences*. 51:193–205.
- Carter L. 1992. Acoustical characterisation of seafloor sediments and its relationship to active sedimentary processes in Cook Strait, New Zealand. *New Zealand Journal of Geology and Geophysics*. 35:289–300.
- Carter L, Carter RM, Nelson CS, Fulthorpe CS, Neil HL. 1990. Evolution of Pliocene to recent abyssal sediment waves on bounty channel levees, New Zealand. *Marine Geology*. 95(2):97–109.
- Carter L, Manighetti B, Elliot M, Trustrum N, Gomez B. 2002. Source, sea level and circulation effects on the sediment flux to the deep ocean over the past 15 ka off eastern New Zealand. *Global and Planetary Change*. 33(3–4):339–355.
- Cartigny MJB, Postma G, van den Berg JH, Mastbergen DR. 2011. A comparative study of sediment waves and cyclic steps based on geometries, internal structures and numerical modeling. *Marine Geology*. 280(1–4):40–56.
- Casciano CI, Patacci M, Longhitano SG, Tropeano M, McCaffrey WD, Di Celma C. 2019. Multi-scale analysis of a migrating submarine channel system in a tectonically-confined basin: The miocene gorgoglione flysch formation, southern Italy. *Sedimentology*. 66(1):205–240.
- Clark IR, Cartwright JA. 2011. Key controls on submarine channel development in structurally active settings. *Marine And Petroleum Geology*. 28(7):1333–1349.
- Collot J-Y, Lewis KB, Lamarche G, Lallemand S. 2001. The giant Ruatoria debris avalanche on the northern Hikurangi margin, New Zealand: result of oblique seamount subduction. *Journal of Geophysical Research*. 106:271–297.
- Cossu C, Wells GW. 2010. Coriolis forces influence the secondary circulation of gravity currents flowing in large-scale sinuous submarine channel systems. *Geophysical Research Letters*. 37(7):1–6.
- Cossu R, Wells MG, Peakall J. 2015. Latitudinal variations in submarine channel sedimentation patterns: the role of Coriolis forces. *Journal of the Geological Society*. 172(2):161–174.
- Crisóstomo-Figueroa A, McArthur AD, Dorrell RM, Amy L, McCaffrey WD. 2020. A new modelling approach to sediment bypass prediction applied to the East Coast Basin, New Zealand. *Geological Society of America Bulletin*. doi:10.1130/B35687.1.
- Damuth JE. 1979. Migrating sediment waves created by turbidity currents in the northern South China Basin. *Geology*. 7(11):520–523.

- Davarpanah Jazi S, Wells MG, Peakall J, Dorrell RM, Thomas RE, Keevil GM, Darby SE, Sommeria J, Viboud S, Valran T. 2020. Influence of coriolis force upon bottom boundary layers in a large-scale gravity current experiment: implications for evolution of sinuous deep-water channel systems. *Journal of Geophysical Research – Oceans*. 125(e2019JC015284):1–30.
- Davy B, Hoernle K, Werner R. 2008. Hikurangi Plateau: crustal structure, rifted formation, and Gondwana subduction history. *Geochemistry, Geophysics, Geosystems*. 9:1–31.
- Denniellou B, Huchon A, Beaudouin C, Berne S. 2006. Vertical grain-size variability within a turbidite levee: autocyclicity or allocyclicity? A case study from the Rhone neofan, Gulf of Lions, Western Mediterranean. *Marine Geology*. 234(1-4):191–213.
- Fernandez D, Bowen MM, Sutton PJH. 2018. Variability, coherence and forcing mechanisms in the New Zealand ocean boundary currents. *Progress in Oceanography*. 165:168–188.
- Flood RD. 1988. A lee wave model for deep-sea mudwave activity. *Deep-Sea Research*. 35:973–983.
- Flood RD, Piper DJW, Klaus A, Burns SJ, Busch WH, Cisowski S, Cramp A, Damuth JE, Goni MA, Haberle SG, et al. 1995. Leg 155 introduction; Amazon Fan. In: Marin JA, editor. *Proceedings of the Ocean Drilling Program, part A: Initial Reports*. Vol. 155. College Station: Texas A & M University, Ocean Drilling Program; p. 5–16.
- Fuhrmann A, Kane IA, Clare MA, Ferguson RA, Schomacker E, Bonamini E, Contreras FA. 2020. Hybrid turbidite-drift channel complexes: An integrated multiscale model. *Geology*. 48(6):562–568.
- Ghissetti FC, Barnes PM, Ellis S, Plaza-Faverola A, Barker DHN. 2016. The last 2 Myr of accretionary wedge construction in the central Hikurangi margin (North Island, New Zealand): insights from structural modelling. *Geochemistry, Geophysics, Geosystems*. 17:2661–2686.
- Hage S, Galy VV, Cartigny MJB, Acikalin S, Clare MA, Gröcke DR, Hilton RG, Hunt JE, Lintern DG, McGhee CA, et al. 2020. Efficient preservation of young terrestrial organic carbon in sandy turbidity-current deposits. *Geology*. 48(9):882–887.
- Hansen LAS, Callow RHT, Kane IA, Gamberi F, Rovere M, Cronin BT, Kneller BC. 2015. Genesis and character of thin-bedded turbidites associated with submarine channels. *Marine and Petroleum Geology*. 67:852–879.
- Hay AE. 1987. Turbidity currents and submarine channel formation in Rupert Inlet, British Columbia; 2, The roles of continuous and surge-type flow. *Journal of Geophysical Research–Oceans*. 92(3):2883–2900.
- Heezen BC, Ewing M, Menzies RJ. 1955. The influence of submarine turbidity currents on abyssal productivity. *Oikos*. 6(2):170–182.
- Hofmann H, Wickham H, Kafadar K. 2017. Letter-value plots: boxplots for large data. *Journal of Computational and Graphical Statistics*. 26(3):469–477.
- Howarth JD, Orpin AR, Kaneko Y, Strachan LJ, Nodder SD, Mountjoy JJ, Barnes PM, Bostock HC, Holden C, Jones K, Cağatay MN. 2021. Calibrating the marine turbidite palaeoseismometer using the 2016 Kaikōura earthquake. *Nature Geoscience*. 14:161–167.
- Jiao R, Seward D, Little TA, Kohn BP. 2015. Unroofing of fore-arc ranges along the Hikurangi Margin, New Zealand: constraints from low-temperature thermochronology. *Tectonophysics*. 656:39–51.
- Kane IA, Clare MA, Miramontes E, Wogelius R, Rothwell JJ, Garreau P, Pohl F. 2020. Seafloor microplastic hotspots controlled by deep-sea circulation. *Science*. 368(6495):1140–1145.
- Kane IA, Hodgson DM. 2011. Sedimentological criteria to differentiate submarine channel levee subenvironments: exhumed examples from the Rosario Fm. (Upper Cretaceous) of Baja California, Mexico, and the Fort Brown Fm. (Permian), Karoo Basin, S. Africa. *Marine and Petroleum Geology*. 28(3):807–823.
- Kane IA, Kneller BC, Dykstra M, Kassem A, McCaffrey WD. 2007. Anatomy of a submarine channel-levee: An example from Upper Cretaceous slope sediments, Rosario formation, Baja California, Mexico. *Marine and Petroleum Geology*. 24:540–563.
- Kane IA, McCaffrey WD, Peakall J. 2008. Controls on sinuosity evolution within submarine channels. *Geology*. 36(4):287–290.
- Kane IA, McCaffrey WD, Peakall J, Kneller BC. 2010. Submarine channel levee shape and sediment waves from physical experiments. *Sedimentary Geology*. 223(1-2):75–85.
- Kao SJ, Dai M, Selvaraj K, Zhai W, Cai P, Chen SN, Yang JYT, Liu JT, Liu CC, Syvitski JPM. 2010. Cyclone-driven deep sea injection of freshwater and heat by hyperpycnal flow in the subtropics. *Geophysical Research Letters*. 37(21):1–5.
- Keevil GM, Peakall J, Best JL, Amos KJ. 2006. Flow structure in sinuous submarine channels: velocity and turbulence structure of an experimental submarine channel. *Marine Geology*. 229(3-4):241–257.
- Kelly RW, Dorrell RM, Burns AD, McCaffrey WD. 2019. The structure and entrainment characteristics of partially confined gravity currents. *Journal of Geophysical Research: Oceans*. 124(3):2110–2125.
- Klaucke I, Hesse R, Ryan WBF. 1998. Seismic stratigraphy of the Northwest Atlantic Mid-Ocean Channel; growth pattern of a mid-ocean channel-levee complex. *Marine and Petroleum Geology*. 15(6):575–585.
- Kneller BC. 1995. Beyond the turbidite paradigm: physical models for deposition of turbidites and their implications for reservoir prediction. In: Hartley AJ, Prosser DJ, editor. *Characterization of deep marine clastic systems*. Geological Society of London Special Publication, Vol. 94. London: The Geological Society of London; p. 31–49.
- Kneller BC, Edwards DA, McCaffrey WD, Moore R. 1991. Oblique reflection of turbidity currents. *Geology*. 19(3):250–252.
- Kneller BC, McCaffrey WD. 1999. Depositional effects of flow nonuniformity and stratification within turbidity currents approaching a bounding slope; deflection, reflection, and facies variation. *Journal of Sedimentary Research*. 69(5):980–991.
- Kroeger KF, Crutchley GJ, Kellett R, Barnes PM. 2019. A 3-D model of gas generation, migration, and gas hydrate formation at a young convergent margin (Hikurangi Margin, New Zealand). *Geochemistry, Geophysics, Geosystems*. 20:5126–5147.
- Kuang Z, Zhong G, Wang L, Guo Y. 2014. Channel-related sediment waves on the eastern slope offshore Dongsha Islands, northern South China Sea. *Journal of Asian Earth Sciences*. 79:540–551.
- Lamb S. 2011. Cenozoic tectonic evolution of the New Zealand plate-boundary zone: A review. *Tectonophysics*. 509:135–164.
- Lewis KB. 1994. The 1500-km-long Hikurangi Channel: trench-axis channel that escapes its trench, crosses a plateau, and feeds a fan drift. *Geo-Marine Letters*. 14:19–28.
- Lewis KB, Barnes PM. 1999. Kaikōura Canyon, New Zealand: active conduit from near-shore sediment zones to trench-axis channel. *Marine Geology*. 162:39–69.

- Lewis KB, Collot JY, Lallemand SE. 1998. The dammed Hikurangi Trough: a channel-fed trench blocked by subducting seamounts and their wake avalanches (New Zealand-France GeodyNZ Project). *Basin Research*. 10:441–468.
- Lewis KB, Pantin HM. 2002. Channel-axis, overbank and drift sediment waves in the southern Hikurangi Trough, New Zealand. *Marine Geology*. 192(1-3):123–151.
- McArthur AD, Tek DE. 2021. Controls on the origin and evolution of deep-ocean trench-axial channels. *Geology*. doi:10.1130/G48612.1.
- McArthur AD, Claussmann B, Bailleul J, McCaffrey WD, Clare A. 2019. Variation in syn-subduction sedimentation patterns from inner to outer portions of deep-water fold and thrust belts: examples from the Hikurangi subduction margin of New Zealand. In: Hammerstein JA, Di Cuija R, Cottam MA, Zamora G, Butler RWH, editor. *Fold and thrust belts: structural style, evolution and exploration* Geological Society of London Special publication, Vol. 490. London: The Geological Society of London; p. 490–545.
- McArthur AD, Bailleul J, Mahieux G, Claussmann B, Wunderlich A, McCaffrey WD. 2021. Deformation-sedimentation feedback and the development of anomalously thick aggradational turbidite lobes: outcrop and subsurface examples from the Hikurangi Margin, New Zealand. *Journal of Sedimentary Research*. 91(4):362–389.
- McArthur AD, Kane I, Bozetti G, Hansen L, Kneller BC. 2020. Supercritical flows overspilling from bypass-dominated submarine channels and the development of overbank bedforms. *The Depositional Record*. 6(1):21–40.
- Menard HW. 1955. Deep-sea channels, topography, and sedimentation. *American Association of Petroleum Geologists Bulletin*. 39(2):236–255.
- Migeon S, Savoye B, Faugeres JC. 2000. Quaternary development of migrating sediment waves in the Var deep-sea fan; distribution, growth pattern, and implication for levee evolution. *Sedimentary Geology*. 133(3-4):265–293.
- Migeon S, Savoye B, Babonneau N, Andersson FLS. 2004. Processes of sediment-wave construction along the present Zaire deep-sea meandering channel: role of meanders and flow stripping. *Journal of Sedimentary Research*. 74(4):580–598.
- Migeon S, Savoye B, Zanella E, Mulder T, Faugeres JC, Weber O. 2001. Detailed seismic-reflection and sedimentary study of turbidite sediment waves on the Var sedimentary ridge (SE France); significance for sediment transport and deposition and for the mechanisms of sediment-wave construction. *Marine and Petroleum Geology*. 18(2):179–208.
- Miramontes E, Eggenhuisen JT, Jacinto RS, Poneti G, Pohl F, Normandeau A, Campbell DC, Hernández-Molina FJ. 2020. Channel-levee evolution in combined contour current–turbidity current flows from flume-tank experiments. *Geology*. 48(4):353–357.
- Mohrig D, Buttles J. 2007. Deep turbidity currents in shallow channels. *Geology*. 35(2):155–158.
- Mountjoy JJ, Barnes PM, Pettinga JR. 2009. Morphostructure and evolution of submarine canyons across an active margin: Cook Strait sector of the Hikurangi Margin, New Zealand. *Marine Geology*. 260(1-4):45–68.
- Mountjoy JJ, Howarth JD, Orpin AR, Barnes PM, Bowden DA, Rowden AA, Schimel AC, Holden C, Horgan HJ, Nodder SD. 2018. Earthquakes drive large-scale submarine canyon development and sediment supply to deep-ocean basins. *Science Advances*. 4(3):eaar3748.
- Morris EA, Hodgson DM, Brunt RL, Flint SS. 2014. Origin, evolution and anatomy of silt-prone submarine external levees. *Sedimentology*. 61(6):1734–1763.
- Muzzi Magalhaes P, Tinterri R. 2010. Stratigraphy and depositional setting of slurry and contained (reflected) beds in the Marnoso-arenacea formation (Langhian-Serravallian) Northern Apennines, Italy. *Sedimentology*. 57(7):1685–1720.
- Nakajima T, Kneller BC. 2013. Quantitative analysis of the geometry of submarine external levees. *Sedimentology*. 60(4):877–910.
- Nakajima T, Satoh M. 2001. The formation of large mudwaves by turbidity currents on the levees of the Toyama deep-sea channel, Japan Sea. *Sedimentology*. 48(2):435–463.
- Nakajima T, Satoh M, Okamura Y. 1998. Channel-levee complexes, terminal deep-sea fan and sediment wave fields associated with the Toyama deep-sea channel system in the Japan Sea. *Marine Geology*. 147(1-4):25–41.
- Nicol A, Mazengarb C, Chanier F, Rait G, Uruski C, Wallace L. 2007. Tectonic evolution of the active Hikurangi subduction margin, New Zealand, since the Oligocene. *TectonicS*. 26:1–24.
- Normark WR. 1970. Growth patterns of deep-sea fans. *AAPG Bulletin*. 54(11):2170–2195.
- Normark WR, Hess GR, Stow DAV, Bowen AJ. 1980. Sediment waves on the Monterey Fan levee; a preliminary physical interpretation. *Marine Geology*. 37(1-2):1–18.
- Normark WR, Piper DJW, Posamentier H, Pirmez C, Migeon S. 2002. Variability in form and growth of sediment waves on turbidite channel levees. *Marine Geology*. 192(1-3):23–58.
- Okon SU, Zhong Q, He Z. 2021. Experimental study on the vertical motion of colliding gravity currents. *Physics of Fluids*. 33(016601):1–11.
- Peakall J, Kane IA, Masson DG, Keevil GM, McCaffrey WD, Corney R. 2012. Global (latitudinal) variation in submarine channel sinuosity. *Geology*. 40(1):11–14.
- Pickering KT, Clark JD, Smith RDA, Hiscott RN, Ricci Lucchi F, Kenyon NH. 1995. Architectural element analysis of turbidite systems, and selected topical problems for sand-prone deep-water systems. In: Pickering KT, Hiscott RN, Kenyon NH, Lucchi FR, Smith RDA, editor. *Atlas of deep water environments; Architectural style in turbidite systems*. London: Chapman and Hall; p. 1–10.
- Piper DJW, Normark WR. 1983. Turbidite depositional patterns and flow characteristics, Navy submarine fan, California Borderland. *Sedimentology*. 30(5):681–694.
- Pirmez C, Flood RD. 1995. Morphology and structure of the Amazon channel. In: Marin JA, editor. *Proceedings of the ocean drilling program, part A: initial reports*. Vol. 155. College Station: Texas A & M University, Ocean Drilling Program; p. 23–45.
- Plaza-Faverola A, Klaeschen D, Barnes PM, Pecher I, Henrys S, Mountjoy J. 2012. Evolution of fluid expulsion and concentrated hydrate zones across the southern Hikurangi subduction margin, New Zealand: An analysis from depth migrated seismic data. *Geochemistry, Geophysics, Geosystems*. 13(8):1–21.
- Pohl F, Eggenhuisen JT, Tilston M, Cartigny MJB. 2019. New flow relaxation mechanism explains scour fields at the end of submarine channels. *Nature Communications*. 10(4425):1–8.
- Ribó M, Puig P, Muñoz A, Lo Iacono C, Masqué P, Palanques A, Acosta J, Guillén J, Ballesteros MG. 2016. Morphobathymetric analysis of the large fine-grained

- sediment waves over the Gulf of Valencia continental slope (NW Mediterranean). *Geomorphology*. 253:22–37.
- Romans BW, Castellort S, Covault JA, Fildani A, Walsh JP. 2016. Environmental signal propagation in sedimentary systems across timescales. *Earth Science Reviews*. 153:7–29.
- Savoie B, Piper DJW, Droz L. 1993. Plio-Pleistocene evolution of the Var deep-sea fan off the French Riviera. *Marine and Petroleum Geology*. 10:550–571.
- Slootman A, Cartigny MJB. 2020. Cyclic steps: review and aggradation-based classification. *Earth-Science Reviews*. 201(102949):1–30.
- Straub KM, Mohrig D, Buttles J, McElroy B, Pirmez C. 2011. Quantifying the influence of channel sinuosity on the depositional mechanics of channelized turbidity currents: A laboratory study. *Marine and Petroleum Geology*. 28(3):744–760.
- Straub KM, Mohrig D, McElroy B, Buttles J, Pirmez C. 2008. Interactions between turbidity currents and topography in aggrading sinuous submarine channels; a laboratory study. *Geological Society of America Bulletin*. 120(3-4):368–385.
- Symons WO, Sumner EJ, Talling PJ, Cartigny MJS, Clare MA. 2016. Large-scale sediment waves and scours on the modern seafloor and their implications for the prevalence of supercritical flows. *Marine Geology*. 371:130–148.
- Tek DE, McArthur AD, Poyatos-Moré M, Colombera L, Patacci M, Craven B, McCaffrey WD. 2021. Relating seafloor geomorphology to subsurface architecture: how mass-transport deposits and knickpoint-zones build the stratigraphy of the deep-water Hikurangi channel. *Sedimentology*. Accepted.
- Timbrell G. 1993. Sandstone architecture of the balder formation depositional system, UK Quadrant 9 and adjacent areas. In: Parker JP, editor. *Petroleum Geology of Northwest Europe: Proceedings of the 4th Conference*. Petroleum Geology Conference series, London, United Kingdom, Vol. 4. London: The Geological Society of London; p. 107–121.
- Watson SJ, Mountjoy JJ, Crutchley GJ. 2020. Tectonic and geomorphic controls on the distribution of submarine landslides across active and passive margins, eastern New Zealand. In: Georgiopoulou A, Amy LA, Benetti S, Chaytor JD, Clare MA, Gamboa D, Houghton PDW, Moernaut J, Mountjoy JJ, editor. *Subaqueous mass movements and their consequences: advances in process understanding, monitoring and hazard assessments*, Geological Society, London, Special publications, Vol. 500. London: The Geological Society of London; p. 477–494.
- Wells M, Cossu R. 2013. The possible role of Coriolis forces in structuring large-scale sinuous patterns of submarine channel-levee systems. *Philosophical Transactions of the Royal Society A – Mathematical Physical and Engineering Sciences*. 371(2004):1–19.
- Wood R, Davy B. 1994. The Hikurangi Plateau. *Marine Geology*. 118:153–173.
- Wynn RB, Stow DAV. 2002. Classification and characterisation of deep-water sediment waves. *Marine Geology*. 192(1-3):7–22.
- Zhong G, Peng X. 2021. Transport and accumulation of plastic litter in submarine canyons—The role of gravity flows. *Geology*. 49(5):581–586.